



# Comparative characteristics and enhanced removal of tetracycline and ceftriaxone by Fe<sub>3</sub>O<sub>4</sub>-lignin and Fe<sub>3</sub>O<sub>4</sub>-carbon-based lignin: Mechanism, thermodynamic evaluation, and DFT calculation



Sunday J Olusegun<sup>a,\*</sup>, Magdalena Osial<sup>a,c</sup>, Taiane G.F. Souza<sup>b</sup>, Michal Krajewski<sup>a</sup>, Gabriel L.S. Rodrigues<sup>d</sup>, Pękała Marek<sup>a</sup>, Pawel Krysinski<sup>a,\*</sup>

<sup>a</sup> Faculty of Chemistry, University of Warsaw, Pasteur Street 1, 02-093 Warsaw, Poland

<sup>b</sup> Department of Metallurgical and Materials Engineering, Universidade Federal de Minas Gerais, Belo Horizonte - MG, Brazil

<sup>c</sup> Department of the Theory of Continuous Media, Institute of Fundamental Technological Research, Polish Academy of Sciences, Pawinskiego 5B Street, 02-106 Warsaw, Poland

<sup>d</sup> Department of Chemistry, School of Engineering Sciences in Chemistry, Biotechnology and Health, KTH Royal Institute of Technology, SE-106 91 Stockholm, Sweden

## ARTICLE INFO

### Article history:

Received 10 October 2022

Revised 29 November 2022

Accepted 12 December 2022

Available online 15 December 2022

### Keywords:

Lignin

Carbon-based lignin, antibiotics

Adsorption mechanisms

Thermodynamics

## ABSTRACT

In this study, eco-friendly Fe<sub>3</sub>O<sub>4</sub>-lignin (FeL) and Fe<sub>3</sub>O<sub>4</sub>-carbon-based lignin (FeCL) were synthesized, characterized, and applied for the adsorption of tetracycline (TRC) and ceftriaxone (CEF). Comparative characterization showed that the BET-specific surface area of FeCL is 27 m<sup>2</sup>/g more than that of FeL. The difference in their morphologies is insignificant, and the particle sizes range between 5 and 15 nm. There is a reduction in the oxygen content and hydroxyl group of FeCL as shown from the EDS and FTIR spectra respectively, compared with FeL. The adsorption capacity for the removal of TRC at 333 K is 156 and 148 mg g<sup>-1</sup> by FeL and FeCL, respectively; while that of CEF are virtually the same. FeL and FeCL adsorption capacity for TRC increases with temperatures (endothermic), but decreases (exothermic) for CEF. The combination of experimental and computational approaches gave insight into the mechanisms of the adsorption process. The mechanisms of TRC and CEF adsorption by FeL and FeCL are the electrostatic attraction, hydrophobic, and  $\pi$ - $\pi$  interaction, while only FeL shows the possibility of hydrogen bond with both TRC and CEF. The study demonstrated that the synthesized material can be reused for up to 3 cycles without an alarming loss of efficiency capacity.

© 2022 Published by Elsevier B.V.

## 1. Introduction

The rise in different bacterial infections has led to increasing production and consumption of antibiotics, leading to their rapid release into the environment. Antibiotics, being one of the most common emerging contaminants that are soluble in aqueous solutions, endanger the lives of different organisms in the ecosystem when present in the soil, surface, and groundwater [1,2]. Numerous sources (such as the pharmaceutical industry, hospital, livestock production, and aquaculture wastewater) of antibiotics in the environment have led to its high-volume pollution load. A study on the toxic effect of antibiotics on the ecosystem showed that it has a negative impact on the photosynthesis activity of plants, while its presence in the soil even in small concentrations could inhibit seed germination, and reduce farmland yields [3–5].

Aside from its effects on plants, it can disrupt the digestive system and cause disturbances in health, also leading to the development of antibiotic resistance by gram-positive and gram-negative bacteria strains [6]. This compromises their effectiveness in treating bacterial infections, thereby resulted to congestion of patients in the hospital and in the worst case increase in death rate. Among such antibiotics are ceftriaxone and tetracycline, which are effective in treating various bacterial infections due to their antimicrobial activities against Gram-positive and Gram-negative bacteria [7,8].

In order to alleviate the negative effects of antibiotics in the environment, an adsorption technique that involves the use of materials (adsorbents) that could effectively remove antibiotics has been proposed. Among these materials are magnetic nanoparticles which have received considerable attention in different fields due to their valuable properties and usefulness for several applications [9]. They are referred to as complex oxides with the crystal structure of a face-centered cubic unit and the general formula of AFe<sub>2</sub>O<sub>4</sub>, while A (divalent cations transition or post-transition metals) and Fe<sup>3+</sup> are arranged in two different crystallographic sites

\* Corresponding authors.

E-mail addresses: [o.sunday@chem.uw.edu.pl](mailto:o.sunday@chem.uw.edu.pl) (S.J Olusegun), [pakrys@chem.uw.edu.pl](mailto:pakrys@chem.uw.edu.pl) (P. Krysinski).

[10]. The position of these cations (A and  $\text{Fe}^{3+}$ ) on tetrahedral or octahedral crystallographic sites determines the formation of spinel ferrites' normal, inverse or mixed lattice structure [11]. Magnetite is an example of inverse spinel ferrites and which eight  $\text{Fe}^{3+}$  cations occupy tetrahedral sites while octahedral sites are occupied by eight of each  $\text{Fe}^{2+}$  and  $\text{Fe}^{3+}$  [12]. Like every other magnetic material, it has been applied to remove contaminants (arsenic, heavy metals, antibiotics, glyphosate, and dyes among others) from wastewater [13–18]. This is credited to their unique properties such as tunable size and shape, high surface-to-volume ratio, chemical stability, surface modifications and can be separated after wastewater treatment through the application of an external magnetic [19]. Magnetite is unique among other oxides due to the presence of Fe in two oxidation states, ferric ( $\text{Fe}^{3+}$ ) and ferrous ( $\text{Fe}^{2+}$ ) [20]. It is the most commonly used naturally occurring iron oxides, which has advantageous features such as high magnetic saturation, biocompatibility, low cost, biodegradability, non-toxicity to humans, and possibility for functionalization [21].

Numerous challenges that are associated with magnetic nanoparticles include (1) the tendency to agglomerate in the aqueous media due to its high surface energy; (2) loss of activity as a result of corrosion/dissolution which depends on the acidity of the environment [19,22]. One of the possibilities to meet the above challenges is to create a magnetite composites or through surface modification. Based on this, the project produced magnetite composites for the removal antibiotics from aqueous solutions.

Lignin is a promising material that can also be used as a matrix for wastewater treatment. It can be combined with magnetite to prevent agglomeration and activity loss, and applied as a magnetic sorbent to remove emerging contaminants. Lignin is a complex macromolecule polymeric material with phenolic hydroxyls, aliphatic, methoxy, carboxylic, and carbonyl functional groups in its chemical structure, which rendered it easy for chemical modification and useful as a stock material [23]. The choice of lignin in this study is due to the presence of abundant hydroxyl groups in its structure which are highly reactive sites, and can be easily modified [24]. Among the sustainable biomass-based polymeric materials, lignin is inexpensive to supply, it is biodegradable and has high carbon content [25].

Carbon material has attracted much attention due to its chemical stability and biocompatibility. Studies have shown that higher lignin content in plants is related to higher carbon content [26]. That makes lignin a potential raw material for the production of various carbon materials. It has been investigated that black carbon, like activated carbon, improved soil fertility and showed affinities for the contaminants [27,28]. Having lignin and carbonized lignin matrix in magnetite will lead to composites with magnetic properties, improved biocompatibility and biodegradability without limitations in the application for the removal of contaminants such as antibiotics.

Given this, this study conducted a comparative study on the synthesis and characterization of  $\text{Fe}_3\text{O}_4$ -lignin and  $\text{Fe}_3\text{O}_4$ -carbon-based lignin, for the removal of ceftriaxone and tetracycline. The adsorption mechanism (through experimental and computational studies) and thermodynamics of the adsorption process were elucidated. Regeneration and reusability through thermal degradation of the adsorbed contaminants were carried out.

## 2. Materials and methods

### 2.1. Materials

Iron(II)chloride tetrahydrate ( $\text{FeCl}_2 \cdot 4\text{H}_2\text{O}$ ), Iron(III)chloride hexahydrate ( $\text{FeCl}_3 \cdot 6\text{H}_2\text{O}$ ), ammonium hydroxide (25 %  $\text{NH}_3$ , assay 99.99 %), and tetracycline hydrochloride (TRC) of analytical grade

were purchased from Sigma-Aldrich, while ceftriaxone (CEF) was obtained from TEUTO Pharma, Brazil. Deionized water with a resistivity of 18.2  $\text{M}\Omega\cdot\text{cm}$  obtained from the Milli-Q ultra-pure water filtering system from Merck was used throughout the experiments. Lignin was supplied by Fibria, Brazil.

### 2.2. Synthesis of magnetite nanocomposites

Magnetite-lignin nanocomposites were synthesized according to the following steps. Firstly, 0.25 g of lignin was added to 25 mL of deionized water inside a 100 mL capacity glass beaker under continuous stirring. Then, 1.35 g of  $\text{FeCl}_3 \cdot 6\text{H}_2\text{O}$  and 0.497 g of  $\text{FeCl}_2 \cdot 4\text{H}_2\text{O}$  were added to the suspension after the dissolution of the iron salts. Co-precipitation of Fe(III) and Fe(II) at alkaline pH was achieved by adding 4 mL of  $\text{NH}_4\text{OH}$ . The precipitate was heated to 90 °C for 1 h, washed until pH is 7, and then, magnetically separated and dried in the oven. The sample is named  $\text{Fe}_3\text{O}_4$ -lignin, and coded as FeL. The content of lignin in  $\text{Fe}_3\text{O}_4$  for sample coded FeL is 30 %. Higher content of lignin (40 and 60 % were also synthesized but based on the preliminary characterization (available in the [supplementary material](#)), 30 % content of lignin was used in this study. Therefore, part of the dried nanocomposites (FeL with 30 % lignin content) was subjected to heating at 500 °C for 2 h under nitrogen gas to produce magnetite-activated carbon derived from lignin, which is named  $\text{Fe}_3\text{O}_4$ -carbon-based lignin, and coded as FeCL.

This particular carbonizing temperature was chosen because the magnetic properties of our composites are of paramount importance for their use in the removal of antibiotics as well as their reusability and regeneration through thermal treatment. Above a certain temperature, called the Curie temperature, magnetite loses its magnetic behavior [29] and cannot be magnetically separated (together with the adsorbed contaminants) from the bulk of the wastewater. In the case of magnetite, this is ca. 583 – 585 °C, and so, 500 °C, is well below the Curie point and is sufficient to carbonize lignin.

Subsequently, both nanocomposites were characterized and used for the removal of ceftriaxone and tetracycline.

### 2.3. Characterization of FeL and FeCL

The  $\text{N}_2$  adsorption/desorption experiments were conducted on Micromeritics® ASAP 2060 apparatus at 77.349 K absolute temperature in the relative pressure range of.

$0.01\text{--}0.995\text{p}(\text{p}^0)^{-1}$ . To analyze the microporosity of the examined magnetite nanocomposites, other experiments were executed, by partially dosing a fixed amount of nitrogen, up to 0.01 relative pressure. Adsorption/desorption isotherm analysis was performed on ASAP 2060 software, by calculating the specific surface area using the BET method, distribution of pores, and their volumes, using the Barret-Joyner-Halenda (BJH) approach for desorption curves and Horvath-Kawazo (H-K) method for micropores examination.

The morphology of FeL and FeCL were examined using a scanning electron microscope (SEM), Merlin, manufactured by Zeiss, equipped with a Gemini II column operated in a low kV value range (0.5–1.5 kV), and probe current 10–20  $\mu\text{A}$ . The range of the particle size of each sample was viewed on transmission electron microscopy (TEM, Zeiss Libra 120 Plus, Stuttgart, Germany, operating at 120 kV). A thermogravimetric analyzer, TGA Q50 (TA Instruments), New Castle, PA, USA, was used to determine the mass loss. This was performed under nitrogen at 60  $\text{cm}^3 \text{min}^{-1}$  flow and oxygen at a 5  $\text{cm}^3 \text{min}^{-1}$  flow rate. The FTIR spectra were recorded with ThermoFisher Scientific Nicolet 8700 spectrometer between 400 and 4000  $\text{cm}^{-1}$ , using a standard KBr method. The magnetic properties of FeL and FeCL were investigated with a QD vibrating

sample magnetometer (VSM) under the magnetic field ranging from  $-2.0$  T to  $+2.0$  T at a temperature of 100 K and 300 K with an accuracy of ca. 0.01 K. Powder X-ray powder diffraction (XRD) was carried out on Bruker D8 Discover with Debye-Scherrer geometry at room temperature with a cobalt  $K\alpha$  X-ray line  $\lambda = 1.7889$  Å, in the  $2\theta$  range from 10 to  $80^\circ$ .

#### 2.4. Adsorption studies

The effect of pH on the adsorption of TRC and CEF was first investigated. Therefore, 5 mg of each adsorbent was added to 7.5 mL of 100 mg/L of the respective adsorbate. The pH of the suspension was adjusted to 2, 4, 6, 8, and 10 using dilute sodium hydroxide and hydrochloric acid. After 24 h, the adsorbents were separated from the antibiotic solutions by applying an external magnet. The concentration of TRC and CEF remaining in the solutions was determined by measuring the absorbance at  $\lambda^{\text{max}}$  357 and 240 nm for TRC and CEF, respectively, using a UV-vis spectrophotometry. Effect of contact time, competing ions and concentrations were also studied. The plots of the kinetic and isotherm were based on the average of the results obtained from the effect of contact time and concentrations at room temperature respectively. Reusability and regeneration of the material through thermal treatment were also carried out.

#### 2.5. DFT calculations

The structures of tetracycline and ceftriaxone were first optimized in gas-phase using the def2-SVP [30] basis sets and the B3LYP [31] exchange–correlation functional. From the optimized structures single-point energy calculations were performed employing a bigger and augmented triple zeta basis set, def2-TZVPD [32,33], while preserving the choice of functional. The reactivity of the molecules were assessed by computing dual descriptor Fukui  $[\Delta f(r)]$  surfaces in its finite difference approximation using the SCF densities of each molecule in its cationic and anionic form according [34,35] to the equation 1:

$$\Delta f(r) = f^+(r) - f^-(r) \quad (1)$$

where  $f^+(r)$  and  $f^-(r)$  are the nucleophilic and electrophilic Fukui functions defined on terms of the electronic density  $\rho(r)$  of a  $N$ -electron molecule as:

$$f^+(r) = \rho_{N+1}(r) - \rho_N(r) \quad (2)$$

$$f^-(r) = \rho_N(r) - \rho_{N-1}(r) \quad (3)$$

All calculations were performed in ORCA (version 5.0.3) employing its default options for each level of theory. The orbital and Fukui function pictures were generated in the Chemcraft program.

### 3. Results and conclusion

#### 3.1. Characterization of $Fe_3O_4$ -lignin (FeL) and $Fe_3O_4$ -lignin-derived carbon (FeCL)

The morphology of the FeL and FeCL obtained from SEM analysis is shown in Fig. 1A and D, respectively. There seems to be an insignificant difference in the morphology of both samples as they display agglomeration of nanoparticles with the presence of intraparticle pores. This also was evident in the nitrogen adsorption/desorption isotherms (showing the presence of hysteresis loop without saturation at higher relative pressures) of both samples as discussed later. TEM images of FeL (Fig. 1B) and FeCL (Fig. 1E) showed clearly that both samples are nanoparticles of spherical

shape with particle size ranging between 5 and 15. There is a slight decrease in the signal of oxygen (O) in the EDS spectrum of FeCL (Fig. 1F) when compared with FeL (Fig. 1C) which was due to the effect of carbonization [36,37].

The isotherms of FeL and FeCL acquired during  $N_2$  adsorption/desorption processes are shown in Fig. 2A. The isotherms are characterized by a mixture of Brunauer's type-II/type-IV isotherm, while the desorption process is mixed H2/H3-type. This behavior suggests a change in the porosity and pore geometry of examined samples, in the direction of more uniform pore size and shape distribution. BET specific surface area ( $BET_{SSA}$ ) calculations showed the highest specific surface area for the FeCL sample, reaching  $112 \text{ m}^2/\text{g}$ , in which  $39 \text{ m}^2/\text{g}$  were attributed to the specific surface area of micropores. While the  $BET_{SSA}$  of FeL is  $85 \text{ m}^2/\text{g}$  with a  $4 \text{ m}^2/\text{g}$  specific surface area of micropores. The reason for high micropores in FeCL could be due to thermal treatment. More so, the carbonization of lignin resulted in a material with an increased affinity for the adsorption of nitrogen gas. Based on the BJH results shown in Fig. 2B, FeL powders showed the smallest mesopore sizes, in the range of 3–6 nm while FeCL it is in the range of 7–10 nm. The zeta potential of the FeL and FeCL are shown in Fig. S1 (Supplementary material).

The BET specific surface area of  $Fe_3O_4$  with 40 and 60 % lignin content are 71 and  $53 \text{ m}^2/\text{g}$  respectively. These values were lower than that of  $Fe_3O_4$  with 30 % lignin. The BET isotherms of  $Fe_3O_4$  with 40 and 60 % lignin content are shown in Fig. S2 (Supplementary material).

Thermal stability analysis of FeL and FeCL shows that FeCL is more thermally stable than FeL since it has been early carbonized. Almost 28 % of the mass was lost from FeL while in the case of FeCL the mass loss was 18 % (due to loss of carbon in the presence of oxygen) as shown in Fig. 2C. However, both samples were stable above  $400^\circ\text{C}$  after all the organic matters (lignin) have been thermally decomposed leaving behind  $Fe_3O_4$ . The mass loss of up to  $200^\circ\text{C}$  is related to the loss of bound water and elimination of humidity [38]. As shown in Fig. 2C, the decomposition process of lignin begins around  $200^\circ\text{C}$  and ends at  $400^\circ\text{C}$ . It is documented in the literature that the thermal decomposition of lignin occurs over a broad range of temperatures due to different oxygen-containing groups that possess different thermal stability [38]. Decomposition of some of these oxygen functional groups could have led to a decrease in oxygen signal in the EDS spectra as shown in Fig. 1C and F.

The TGA plots of  $Fe_3O_4$  with 40 and 60 % lignin content are shown in Fig. S3 (Supplementary material). The results confirmed the respective amount, 40 and 60 % lignin content that were added to  $Fe_3O_4$ .

The FTIR of FeL and FeCL is presented in Fig. 2D. There are obvious changes in the spectra of the FeL after transformation to FeCL. Firstly the peak at  $3412 \text{ cm}^{-1}$  on the spectrum of FeL, which is attributed to the stretching vibration of  $-\text{OH}$  groups from phenolic, disappeared after carbonization, with the appearance of almost a flattened band at  $3320 \text{ cm}^{-1}$  on the spectrum of FeCL due to dehydroxylation. The disappearance of this peak could be due to water loss during the carbonization as shown in TG analysis. The peak at  $2928 \text{ cm}^{-1}$  with low intensity, is attributed to the vibration of  $-\text{CH}$  from  $-\text{CH}_2$  groups of lignin [39]. This peak disappeared after carbonization, which probably could be due to a reduction reaction that occurred during calcination resulting in loss of hydrogen atoms and decomposition of volatile groups in lignin. The absorption peaks at  $1610$  and  $1514 \text{ cm}^{-1}$  are assigned to aromatic skeletal vibrations from lignin [40]. The aftermath of calcination is a shift of the sharp peak at  $1610 \text{ cm}^{-1}$ , to  $1590 \text{ cm}^{-1}$  as it can be seen on the spectrum of FeCL, while  $1514 \text{ cm}^{-1}$  disappeared. The sharp peaks at  $1217$  and  $1113 \text{ cm}^{-1}$  are characteristic to the presence of CO stretching vibration of guaiacyl ring breathing [39,40], which

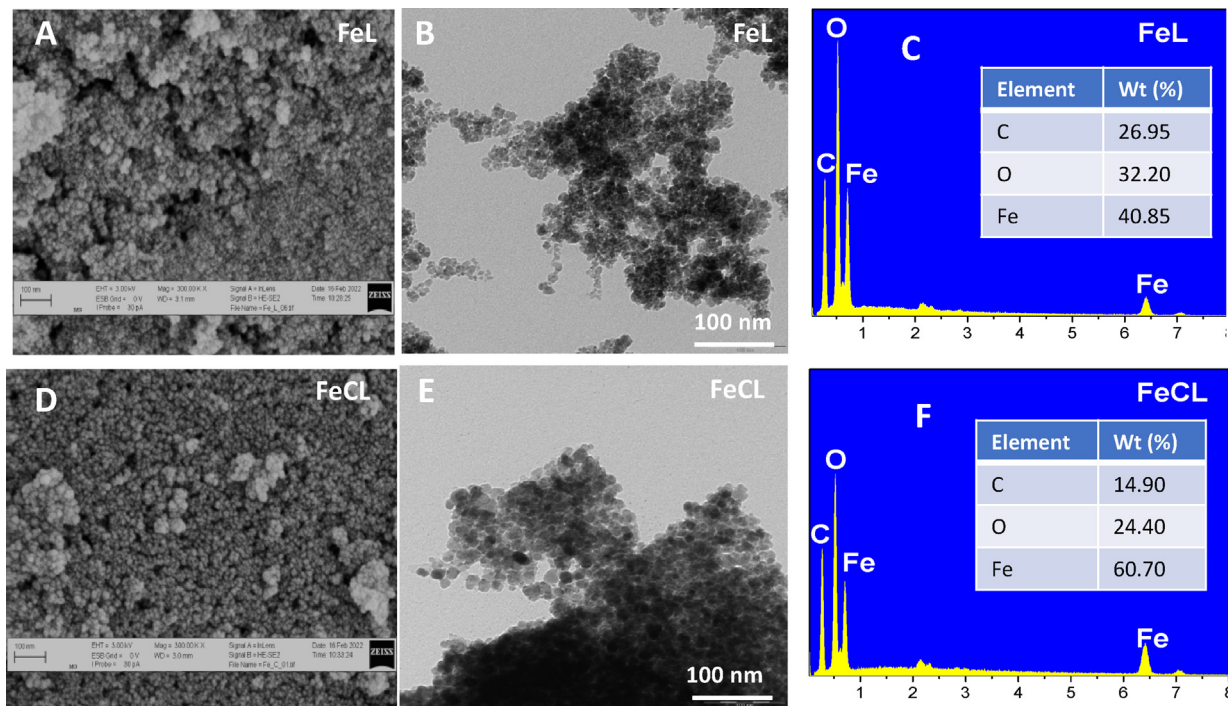


Fig. 1. SEM images (A and D); TEM images (B and E) and EDS spectra (C and F) of FeL and FeCL.

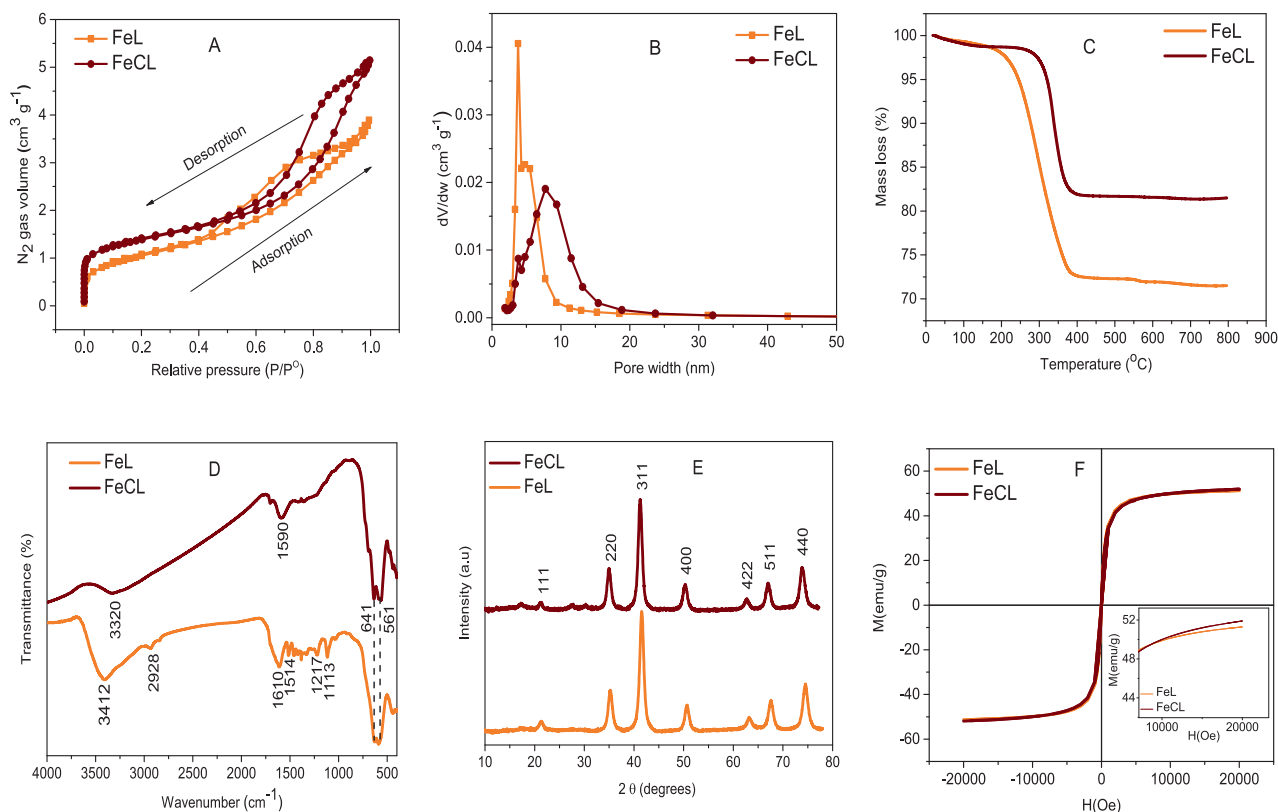


Fig. 2. Nitrogen adsorption/desorption (A); BJH (B); TGA (C); FTIR (D); the diffractogram (E) and magnetization (at room temperature) versus applied field (F) of FeL and FeCL.

disappeared after carbonization. The disappearance of CO and a drastic reduction in the intensity –OH groups was paralleled in reduction in the O signal as shown in the EDS of FeCL in Fig. 1 C and F. Lastly, the two peaks at 641 and 561 cm<sup>-1</sup> are characteristic fingerprint of iron oxides [41].

The diffractograms of the FeL and FeCL showed in Fig. 2E match with ICSD Number: 029129, which is evidence that the synthesized samples are magnetite. The diffractogram is similar to that magnetite which was done using cobalt cathode as reported by Peternele et al. [42]. There is no reflection of lignin and lignin-based

activated carbon since they are amorphous materials of low intensity. The crystallite size calculated from Scherrer equation at  $2\theta$ ,  $41.5^\circ$  being the peak with the highest intensity are 9.35 and 9.63 nm for FeL and FeCL, respectively.

The magnetization curves  $M(H)$  at room temperature are presented in Fig. 2F. The plots of both samples partially overlap. However, the inset shows a slight difference in the magnetic saturation of both samples where magnetic saturation (Ms) values of 51.7 and 52.4  $\text{emu g}^{-1}$  are achieved for FeL and FeCL, respectively. These close Ms values confirm that the nanocrystallite size does not increase during their thermal treatment at  $500^\circ\text{C}$  (compare the XRD results in Fig. 2E). The value of magnetization, however, is lower than that for the bulk  $\text{Fe}_3\text{O}_4$  (92  $\text{emu/g}$ ). The Ms reduction occurs due to the structural disorder as well as the presence of lignin and activated carbon that would have caused a magnetic dead layer in the magnetic nanocrystallites. Both samples exhibit remarkably low magnetic coercivity. At room temperature, the coercive fields ( $H_c$ ) derived from hysteresis loops are equal to 0.5 and 9 Oe for FeL and FeCL, respectively. Such low coercive fields  $H_c$ , as well as the shape of the magnetization curve  $M(H)$ , are the characteristic features of superparamagnetic (magnetic monodomain) materials. More so the magnetic remanence is less than 2  $\text{emu g}^{-1}$  for both samples. These low  $H_c$  values connote that there will be a quick loss of magnetic memory after the withdrawal of an external magnetic field. The magnetic saturation of  $\text{Fe}_3\text{O}_4$  with 40 and 60 % lignin content are 47.7 and 39.8  $\text{emu g}^{-1}$  respectively (Fig. S4 (Supplementary material)). These values are lower than  $\text{Fe}_3\text{O}_4$  with 30 % lignin content.

### 3.2. Effect of solution pH on the adsorption of TRC and CEF

Solution pH is one of the factors that could affect the adsorption of contaminants. It affects the ionization of adsorbate and the adsorbent's surface charge. To understand the adsorption of TRC and CEF by FeL and FeCL at different pH, studies were performed on pH ranging from 2, 4, 6, 8, and 10. Before this, the zeta potential of the two adsorbents was measured, and the isoelectric point (IEP) was determined. The IEP of FeL and FeCL are found to be 3.4 and 3.3 (supplementary material). The results obtained from the effect of solution pH are shown in Fig. 3. The amount of TRC that FeL adsorbed increased from 19  $\text{mg g}^{-1}$  at pH 2 to 41  $\text{mg g}^{-1}$  at pH 6, after which it declined significantly at pH 8 and 10. The trend was different for FeCL, the amount increases with an increase in pH. However, there is no significant increase in the amount adsorbed from pH 6 to 10. Compared to FeL, 50  $\text{mg g}^{-1}$  of TRC

was adsorbed by FeCL at pH 6. Further comparison shows that FeCL adsorbed TRC better than FeL within the studied pH and concentration. That could be credited to its specific surface area that is higher than that of FeL. Depending on the solution pH, TRC occurs in different ionization forms. At pH less than 3, it is being protonated, and occurs majorly in cationic form, while at pH between 3 and 7, zwitterionic. As the solution pH becomes alkaline, it becomes deprotonated, leading to the existence of anionic species [41,43]. Therefore, the small adsorption of TRC on FeL at pH 2 results from electrostatic repulsion between the positively charged surface of FeL and the cationic form of TRC. This repulsion also occurred at pH 8 and 10, since both FeL and TRC are negatively charged. However, at pH 4 and 6, the presence of TRC  $\pm$  favors the electrostatic attraction between the cationic part of TRC and the negatively charged surface of FeL. However, the adsorption mechanism of TRC by FeL is not limited to electrostatic interaction. In the case of FeCL, a significant amount was adsorbed within the studied pH, which means that the electrostatic repulsion was suppressed by other adsorption mechanisms that favored the adsorption of TRC.

The adsorption of CEF by both FeL and FeCL as shown in Fig. 3B follows a pattern different from that of TRC, in the sense that it decreases with an increase in solution pH. Different species of CEF ( $\text{H}_3\text{C}^+$ ,  $\text{H}_2\text{C}^+$ , and  $\text{HC}^{2+}$ ) exist in an acid medium, having three acid dissociation constants:  $\text{pK}_1 = 2.37$  (COOH),  $\text{pK}_2 = 3.03$  (aminothiazole), and  $\text{pK}_3 = 4.21$  (hydroxytriazinone) [44]. That implies that at pH 2, the electrostatic attraction between the positively charged FeL and FeCL and the anionic form of CEF favored the adsorption process. Despite the electrostatic repulsion at alkaline pH, some reasonable amount of CEF was adsorbed, which implies that other adsorption mechanisms are involved, similarly as in the case of TRC. In general, FeCL adsorbed both contaminants more than FeL due to the high specific surface area as earlier discussed. However, when the amount at pH 6 for TRC and pH 4 for CEF was normalized by the specific surface area the results obtained are 0.49, 0.45, 0.65, 0.56  $\text{mg m}^{-2}$  for FeL-TRC, FeCL-TRC, FeL-CEF, and FeCL-CEF respectively. The values for FeL being higher than that of FeCL for the two antibiotics show that the amount adsorbed is not solely related to the specific surface area of each material but the nature of the adsorption sites. We could recall that out of the 112  $\text{m}^2/\text{g}$  of FeCL, 39  $\text{m}^2/\text{g}$  were attributed to micropores while 4  $\text{m}^2/\text{g}$  of 85  $\text{m}^2/\text{g}$  of FeL were due to the presence of micropores. That could be the reason why normalized values of the amount adsorbed in the case of FeL are greater than those in the case of FeCL, since the adsorption of antibiotics whose molecules

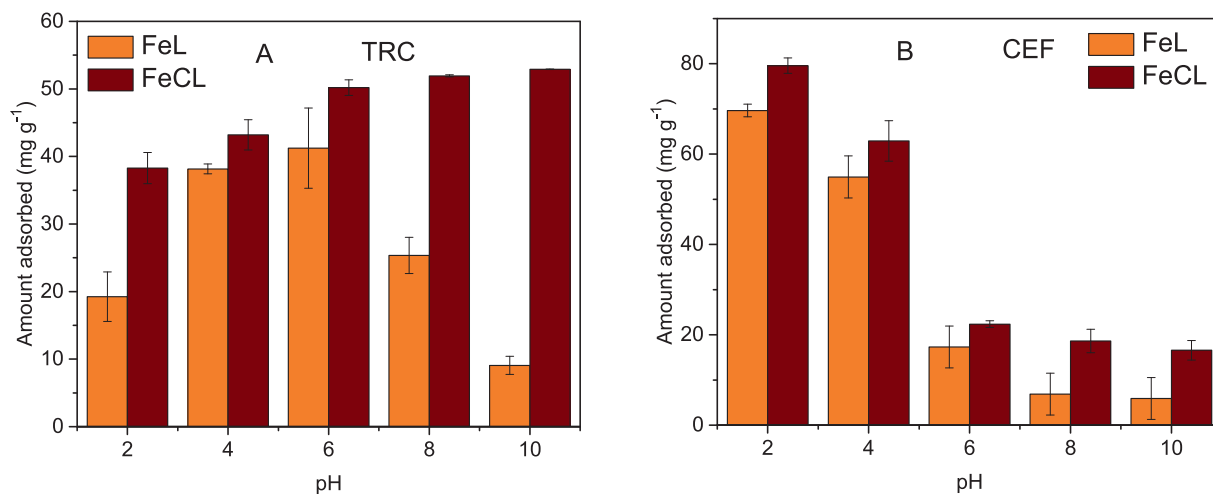


Fig. 3. Effect of pH on the adsorption of TRC and CEF.

are relatively large are favored by mesoporous materials [45]. The rest study was undertaken at pH 4 for CEF since pH 2 is too acidic for the dissolution of iron oxides.

### 3.3. Adsorption kinetics for the removal of CEF and TRC by both FeL and FeCL

The study of contact time/kinetics was carried out using 50 mg/L of TRC and CEF respectively. As shown in Fig. 4, approximately 50 % of each of the adsorbate was removed after 1 h of contact time. The availability of the active sites on the surface of FeL and FeCL hastened the adsorption of TRC and CEF. At this initial stage, the high concentration of the molecules of TRC and CEF in the bulk solution, could facilitate their diffusion to the surface of the FeL and FeCL, resulting to rapid adsorption at the early stage. After 1 h of contact time the adsorption process was a bit low since some of the adsorption sites have been occupied. This low adsorption process continue until equilibrium was attained between 8 and 9 h. The data obtained were further treated by applying pseudo-first order, pseudo-second order, and Elovich kinetic models (The non-linear equations of the models are available at the Supplementary Material). Basically, the value of  $R^2_{adjusted}$  and SD provide information on the model that is more appropriate to describe the kinetics of the adsorption process. The values of their parameters

are listed in Table 1S of the Supplementary Material. The values of  $R^2_{adjusted}$  obtained from Elovich model are higher than that of pseudo-first order and pseudo-second order. Elovich is related to chemisorption kinetic process, bulk and surface diffusion of the adsorbates [46].

### 3.4. Adsorption isotherms

The adsorption isotherms provide information about the equilibrium behavior of a material (adsorbents) at the various concentration of the contaminants (adsorbates), at the fixed mass of the adsorbent, and a given temperature. Different adsorption models have been developed to study the experimental data and predict the best isotherm equations describing the adsorption process. These equations are given as the plot of the amount adsorbed at equilibrium versus the equilibrium amount of the adsorbates in the solution at a constant solution pH, volume, temperature and amount of adsorbent. Langmuir and Freundlich isotherms are among the models frequently used to describe the adsorption process. One of the ways to choose the best model that is appropriate to describe the mode of adsorption of the contaminants on the adsorbent is through the determination of the coefficient ( $R^2_{adjusted}$ ), being a statistical measure of fit that indicates how much variation of a dependent variable ( $q_e$ ) is

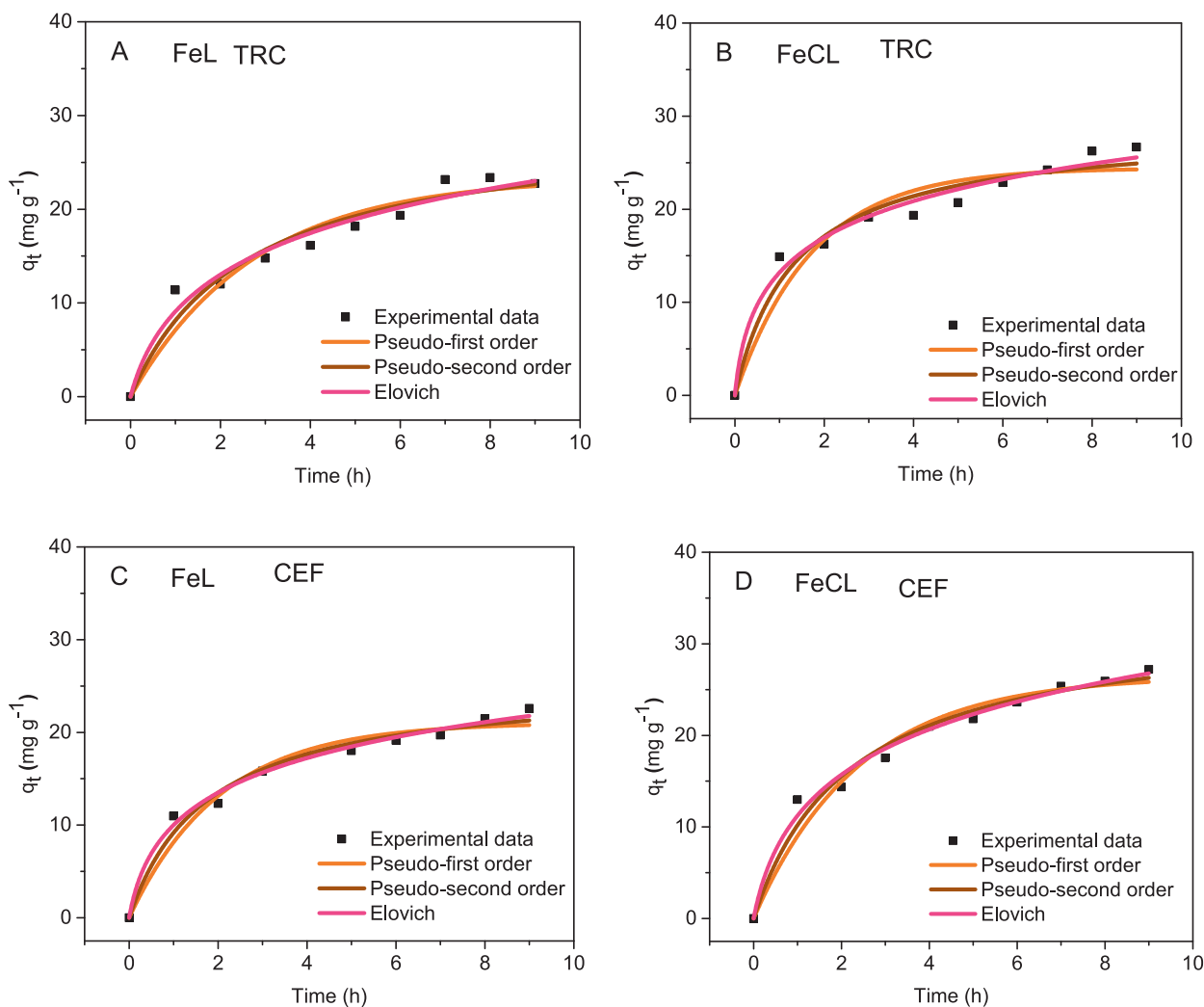


Fig. 4. Kinetic models for the removal of TRC and CEF.

**Table 1**  
Langmuir and Freundlich isotherms parameters for the adsorption of TRC at 298, 313 and 333 K.

	FeL			FeCL		
	298 K	313 K	333 K	298 K	313 K	333 K
Langmuir						
$q_{max}$ (mg/g)	59	149	156	61	125	148
$K_L$ (L/mg)	0.068	0.122	0.202	0.122	0.371	0.219
$R^2_{adjusted}$	0.978	0.948	0.821	0.965	0.955	0.965
SD (mg g <sup>-1</sup> )	2.51	10.91	22.60	3.48	9.21	9.39
Freundlich						
$K_F$ (mg/g (mg/L) <sup>-1/nF</sup> )	15.58	42.94	54.42	20.12	49.48	49.43
$n_F$	3.94	3.79	4.25	4.45	4.67	3.98
$R^2_{adjusted}$	0.938	0.851	0.793	0.981	0.946	0.942
SD (mg g <sup>-1</sup> )	4.28	18.52	24.30	2.58	10.14	12.76

explained by the independent variable ( $c_e$ ) in an isotherm model, and the standard deviation (SD).

The non-linear forms of these isotherms' equations are available in the [supplementary material](#) while their curve fits at different temperatures, are presented in Fig. 5. The parameters of the isotherms for the adsorption of TRC and CEF are listed in [Tables 1 and 2](#), respectively. Going by the highest values of  $R^2_{adjusted}$  and lowest of SD, the adsorption process of TRC and CEF is well explained by the isotherm model that was proposed by Langmuir, which

defined the homogenous adsorption of adsorbates (TRC and CEF) on the adsorbents (FeL and FeCL). The theoretical adsorption capacity ( $q_{max}$ ) increases with the rise in temperature for TRC, while it decreases for CEF. The implication of this was discussed in the section below. Comparison between  $q_{max}$  reported in the literature with what was obtained in this study, are shown in [Table 3](#). FeL and FeCL performed better than some reported adsorbents in the literature; this makes them an effective material for the removal of TRC and CEF from aqueous solutions.

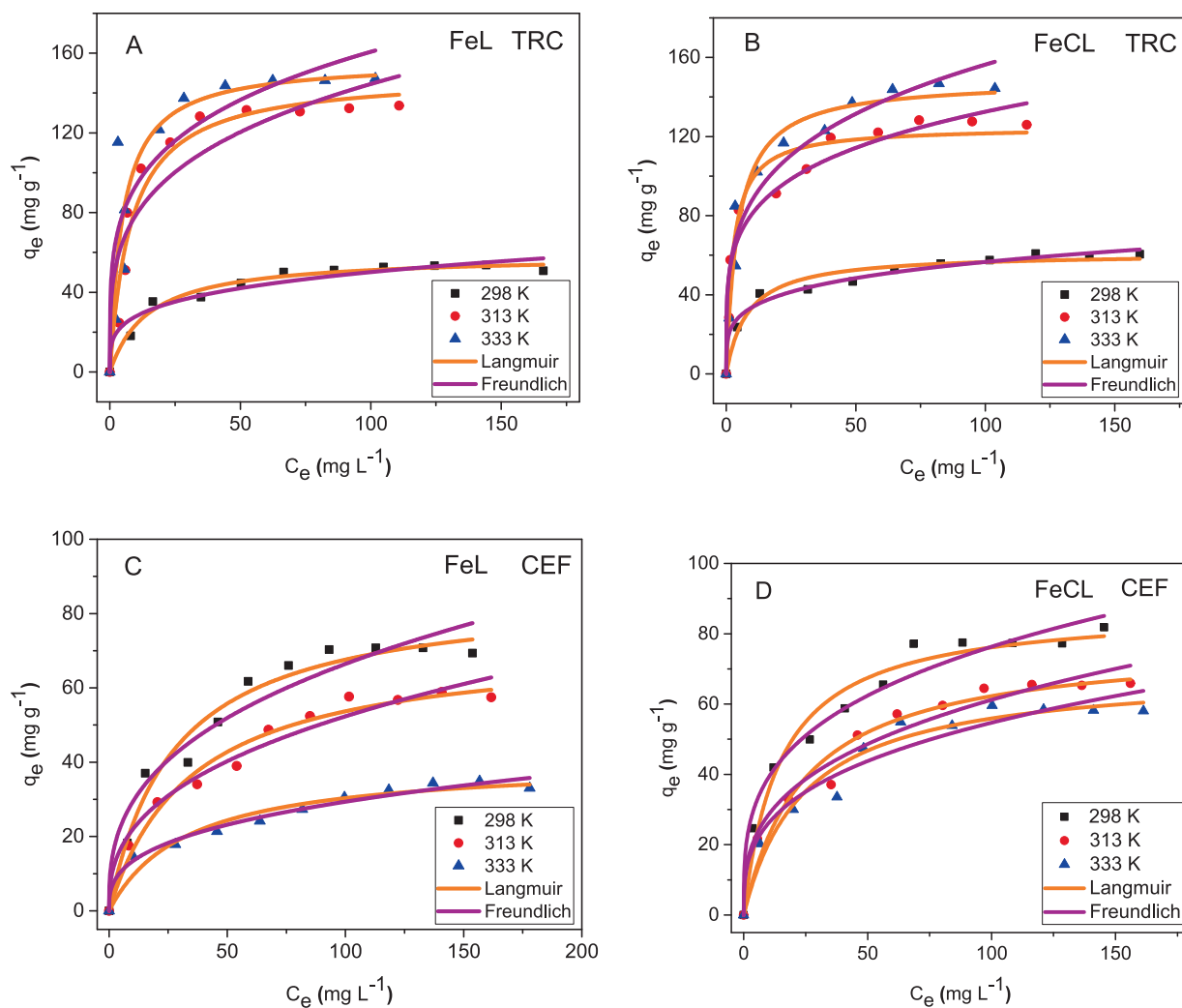


**Fig. 5.** Adsorption isotherms for the removal of TRC and CEF at different temperatures.

**Table 2**  
Langmuir and Freundlich isotherms parameters for the adsorption of CEF at 298, 313 and 333 K.

	FeL			FeCL		
	298 K	313 K	333 K	298 K	313 K	333 K
Langmuir						
$q_{max}$ (mg/g)	86	72	40	87	78	70
$K_L$ (L/mg)	0.037	0.029	0.031	0.067	0.041	0.041
$R^2_{adjusted}$	0.974	0.979	0.959	0.969	0.966	0.956
SD	4.06	2.91	2.26	4.604	3.980	4.094
Freundlich						
$K_F$ (mg/g (mg/L) <sup>-1/nF</sup> )	12.89	9.14	6.07	20.02	13.27	12.47
$n_F$	2.809	2.639	2.922	3.44	3.01	3.11
$R^2_{adjusted}$	0.944	0.971	0.981	0.975	0.967	0.943
SD	5.69	3.25	1.45	4.10	3.95	4.69

**Table 3**  
Comparison of the maximum adsorption ( $q_{max}$ ) of different adsorbents for the removal of TRC and CEF.

Contaminants	Adsorbents	$q_{max}$ (mg/g)	References
Tetracycline	Fe <sub>3</sub> O <sub>4</sub> @C	14	[47]
	Hydrous ferric oxide	41	[48]
	R600	14	[49]
	FeMn-BC	14.24	[50]
	Cu-immobilized alginate	58	[51]
	Magnetic porous carbon	25	[52]
	Zn/Fe/La LDH	170	[53]
	FeL	156	This work
	FeCL	148	This work
	Ceftriaxone	PAC-MNPs	28
(NTiO <sub>2</sub> -Chit)		90	[55]
Clinoptilolite		0.0058	[56]
150FeOH		57	[57]
Saccharomyces Cerevisiae		12	[58]
Fh-0 %Si		125	[59]
FeL		85	This work
FeCL		87	This work

So far, these results demonstrated a strong interaction between TRC and the adsorbents (FeL and FeCL) in which the adsorbed molecules could not be desorbed as the temperature increases. It also shows that the equilibrium between adsorption and desorption was shifted and favored adsorption of TRC as the temperature increased. According to El Kady et al., [60], the role of temperature in the adsorption of contaminants cannot be underestimated because it creates new binding sites for the adsorption of the targeted molecules and increases the mobility of the adsorbate molecules.

As shown in Fig. 6B the adsorption capacity of FeL and FeCL for CEF decreases with an increase in temperature. As the temperature increases, the tendency of the weakly adsorbed CEF molecules to leave the surface of the two adsorbents increases thereby reducing the amount adsorbed.

More insights were gained into the adsorption of TRC and CEF by calculating the thermodynamic parameters using equations (2) – (4). The first step was converting the Langmuir adsorption equilibrium ( $K_L$ ) constant to a dimensionless unit as shown in equation (2) [61], then calculating Gibbs free energy changes ( $\Delta G^\circ$ ), enthalpy changes ( $\Delta H^\circ$ ), entropy changes ( $\Delta S^\circ$ ) by using Van't Hoff and Gibbs-Helmholtz equations as shown in equations (3) and (4).

$$K_e = \frac{1000 * K_L * \text{molecular weight of the adsorbate} * \text{standard concentration of the adsorbate}}{\text{activity coefficient of adsorbate}} \tag{2}$$

### 3.5. The influence of temperature, and thermodynamics of the adsorption

The influence of rise in temperature on the adsorption capacity of FeL and FeCL for the removal of TRC and CEF are presented in Fig. 6A and B. As shown in Fig. 6A an increase in temperature of the aqueous solution of TRC resulted in an increase in the amount removed by both FeL and FeCL. That could be explained that as the temperature increases, TRC molecules gain more kinetic energy, which hastens their mobility towards the two adsorbents and thereby adsorbed. Wang et al., [49], reported a similar observation for the adsorption of tetracycline using biochar derived from rice straw. These authors commented that the more energy that tetracycline gains with an increase in temperature, the larger the number of these molecules that will interact with the adsorption sites, thereby favoring the adsorption capacity of the adsorbent.

The standard concentration of any molecule or ion is 1 mol/L, while the activity coefficient is also 1 [61].

$$\log K_e = \frac{\Delta S^\circ}{2.303R} - \frac{\Delta H^\circ}{2.303RT} \tag{3}$$

$$\Delta G^\circ = \Delta H^\circ - T\Delta S^\circ \tag{4}$$

Listed in Table 4 are the thermodynamic parameters for the adsorption of the TRC and CEF. Changes in enthalpy for removing TRC by both FeL and FeCL are positive. It followed the results displayed in Fig. 6. The positive values indicate an endothermic reaction in which an increase in temperature favors the adsorption removal of TRC. The adsorption and removal of CEF by the two adsorbents is a slightly exothermic process; since the values of  $\Delta H^\circ$  are negative; the adsorption is favored at lower temperatures. The changes in entropy for TRC and CEF are both positive.

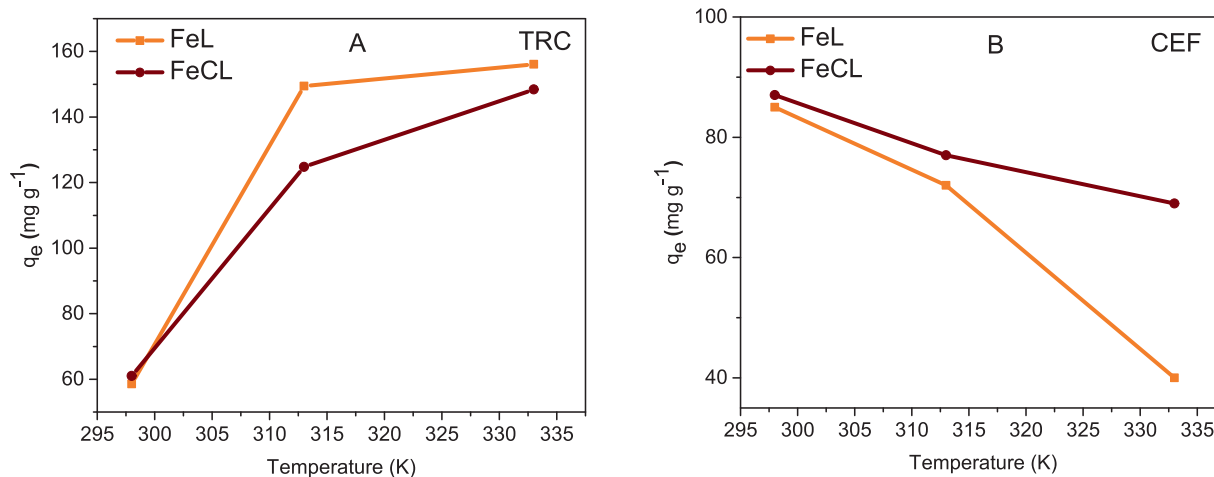


Fig. 6. Influence of temperature on the adsorption of; (A): TRC and (B): CEF.

Table 4  
Thermodynamic parameters.

Adsorbents	Adsorbates	$\Delta H^{\circ}$ (kJ/mol)	$\Delta S^{\circ}$ (J/K mol <sup>-1</sup> )	$\Delta G^{\circ}$ (kJ/mol)		
				298 K	313 K	333 K
FeL	TRC	25.52	172.41	-25.85	-28.43	-31.88
FeCL		12.62	136.21	-27.96	-30.00	-32.73
FeL	CEF	-4.74	66.20	-24.47	-25.46	-26.79
FeCL		-11.46	48.27	-25.84	-26.57	-27.53

Therefore, there is an increase in the randomness in the adsorption process at the solid and solution interface [62]. Irrespective of the endothermic and exothermic adsorption process for TRC and CEF, respectively, the removal of the two antibiotics is spontaneous in all the temperatures studied, because of negative values of the Gibbs's free energy of adsorption.

### 3.6. Effect of competing ions (Na<sup>+</sup>, Cl<sup>-</sup>, H<sub>2</sub>PO<sub>4</sub><sup>-</sup>)

The presence of salt cannot be ruled out in wastewater; given this, the influence of NaCl on the adsorption of TRC and CEF was investigated. It is evident from the results shown in Fig. 7A and B, that presence of Na<sup>+</sup>, and Cl<sup>-</sup> did not have a significant negative effect on the removal of the studied antibiotics. This makes it advantageous to use FeL and FeCL for the removal of TRC and CEF from aqueous solutions that contain salts. The slight decrease in the amount of CEF adsorbed by the two adsorbents is evidenced by the outer-sphere complexation, whereas that of TRC implies that the interaction between the two adsorbates and the adsorbents is an inner-sphere complexation [63]. In the inner-sphere complexes, the presence of background electrolyte does not affect the adsorbed contaminants, whereas it reduces the adsorption of contaminants in outer-sphere complexes [63]. The slight increase in the amount of TRC that adsorbed at higher concentration of the ionic strength is due to the salting-out effect, in which the addition of salt slightly reduces the solubility of TRC, thereby leading to an increasing the adsorption of its molecules[64]. More so, non-electrostatic forces such as hydrophobic interactions are responsible for an increase in the amount of organic contaminants adsorbed with increasing ionic strength [65].

Phosphates is essential for the growth and development of both animals and plants. However, it is regarded as pollutant when they are in excess in surface water [66,67]. Depending on the solution

pH (pK<sub>1</sub> 2.2, pK<sub>2</sub> 7.2, pK<sub>3</sub> 12.3), phosphates exist in different forms (H<sub>3</sub>PO<sub>4</sub>, H<sub>2</sub>PO<sub>4</sub><sup>-</sup>, HPO<sub>4</sub><sup>2-</sup> or PO<sub>4</sub><sup>3-</sup>) [68]. The adsorption of TRC and CEF under the effect of competing ions were carried out at pH 4 and 6 respectively being the optimum pH determined in the preceding experiments (vide supra). It is reported that H<sub>2</sub>PO<sub>4</sub><sup>-</sup> is the major phosphate species at pH 2 – 7 [69]. The choice of phosphates as competing (H<sub>2</sub>PO<sub>4</sub><sup>-</sup>) is based on the fact that the discharge of antibiotics into the environment leads to their interaction with soil, sediments, surface, and groundwater. At the same time, phosphates are being drained into surface water from industries, and the agricultural sector (through the use of chemical fertilizers) [70].

As it can be seen in Fig. 7C and D, the presence of H<sub>2</sub>PO<sub>4</sub><sup>-</sup> could not significantly reduce the amount of TRC and CEF that were adsorbed by the two adsorbents. That could occur due to electrostatic repulsion between FeL and FeCL that is negatively charged at the studied pH and H<sub>2</sub>PO<sub>4</sub><sup>-</sup>. Since phosphates interact with iron (hydr)oxides by electrostatic interaction as well as through complexation, the slight reduction in the amount of TRC and CEF in the presence of phosphate could be due to the complexation of magnetite with phosphate ions. The adsorption of an antibiotic levofloxacin, by goethite (FeOOH) in the presence of phosphate in the solution pH less than 7, was retarded significantly, as reported by Qin et al [71]. This was credited to the complexation of phosphate ion with the two hydroxyl groups on the goethite surface, leading to the unprotonated bidentate phosphate-goethite complex ( $\equiv \text{Fe}_2\text{O}_2\text{PO}_2$ ). The coating of lignin and carbon-based lignin on the magnetite used in our study, coupled with limited hydroxyl groups inhibits the complexation process; hence, low impact on the adsorption of the TRC and CEF was recorded. However, when the phosphate concentration was 80 and 100 mg/L, the amount of the two antibiotics begin to pick up, which is higher than the amount adsorbed at 20, 40, and 60 mg/L, although not up to the amount removed without the addition of phosphate. That could

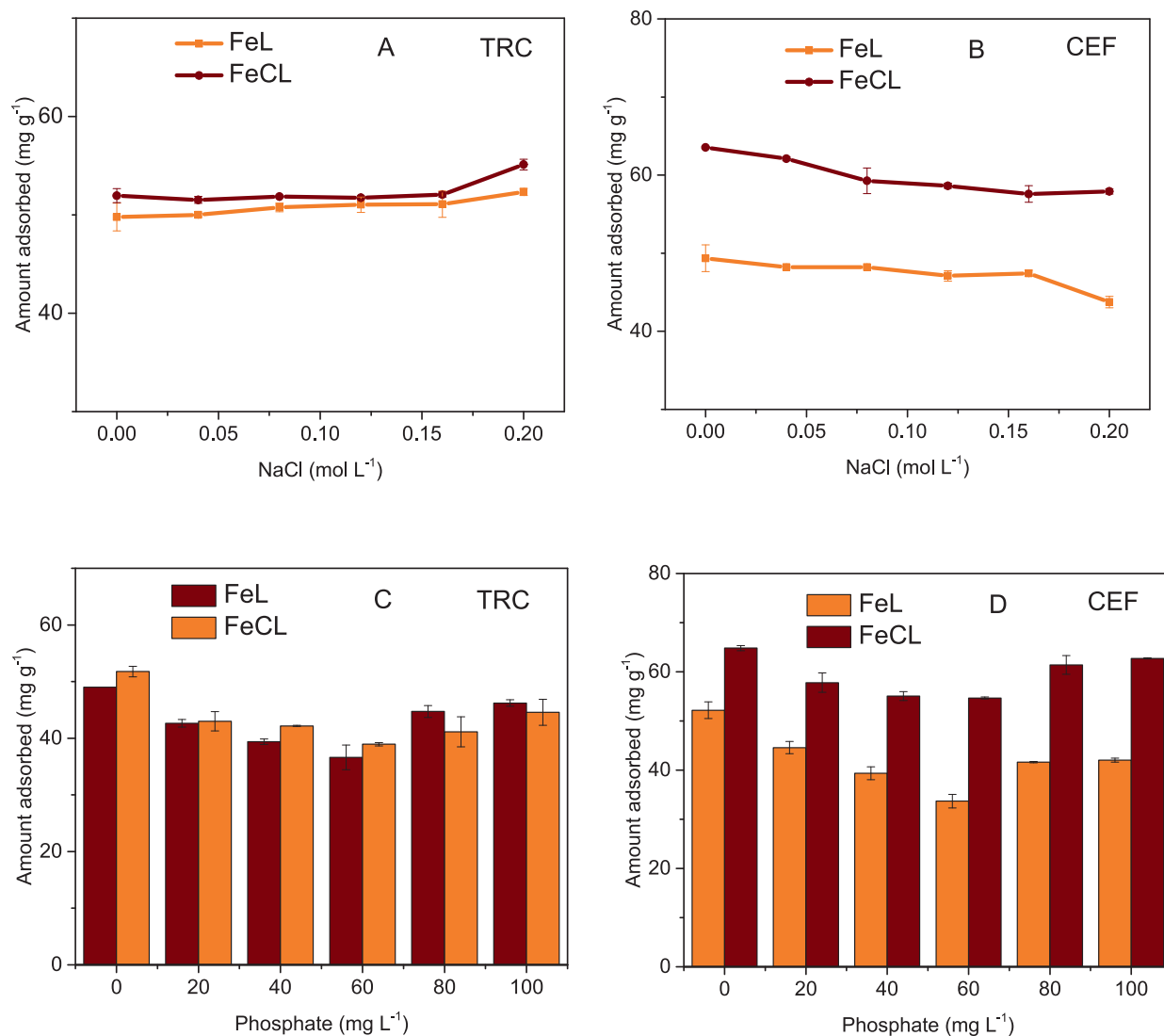


Fig. 7. Effect of NaCl (A and B) and phosphate (C and D) on the adsorption of TRC and CEF.

be credited to hydrophobic interactions in which the addition of salts at higher concentrations favored the adsorption of organic molecules by reducing their solubility in aqueous solutions. According to McCue, 2009 [72], the strength of anions with respect to hydrophobic interaction between organic molecules differs. He added that phosphate anion tends to increase hydrophobic interaction more than chloride anions.

### 3.7. Proposed adsorption mechanism

The FTIR technique is one of the techniques used to understand the interaction between adsorbent and adsorbate and to guide in establishing the adsorption mechanisms. The FTIR spectra of FeL and FeCL after adsorption of TRC are presented in Fig. 8A, with the enlarged range of the spectra in Fig. 8B. Starting with the hydroxyl group of FeL at  $3412\text{ cm}^{-1}$ , the large and broad peak before adsorption was broader and smaller after the adsorption of TRC. This effect implies the participation of hydroxyl groups and could be the consequence of hydrogen bond interaction between TRC and the FeL. More so, the intensity of the peak at  $1613\text{ cm}^{-1}$  increased after adsorption. This peak was initially at  $1610\text{ cm}^{-1}$  (see section 3.1), and it is related to aromatic skeletal

vibrations from lignin, at the same time the  $\text{-C=O}$  group of TRC is located at  $1611\text{ cm}^{-1}$  [53]. In the case of FeCL + TRC there is a new peak at  $1613\text{ cm}^{-1}$ , while the initial peak at  $1590\text{ cm}^{-1}$  shifted to  $1560\text{ cm}^{-1}$ . These observations for the two adsorbents implies that a linkage could occur through the O atom in  $\text{-C=O}$  and the aromatic skeletal of FeL and FeCL, leading to  $\pi$ - $\pi$  interaction.

Examining the spectra of FeL and FeCL after the adsorption of ceftriaxone (Fig. 8C), the peak at  $3412\text{ cm}^{-1}$  on the spectrum of FeL that signifies the presence of OH, became broader after adsorption of CEF. Furthermore, the shaded part on FeL and FeL + CEF in Fig. 8 contain characteristic peaks of vibration deformation in the C-H bond at  $1372\text{ cm}^{-1}$  and the stretching of C-O (ether) of lignin at  $1114\text{ cm}^{-1}$ . It is visible that both peaks significantly change on FeL + CEF, clearly showing absorption of CEF.

There is no obvious changes in the OH of FeCL after adsorption. On the other hand, the intensity of peak at  $1590\text{ cm}^{-1}$  (C=C, aromatic skeletal) on the shaded part of FeCL and FeCL + CEF was reduced significantly after adsorption, the sharp peak of FeL at  $1610\text{ cm}^{-1}$  was broadened after adsorption (FeL + CEF) these observations connote change in the aromatic ring electronic structure through  $\pi$ - $\pi$  interactions [73]. Further insight on the mechanisms were obtained from DFT calculations.

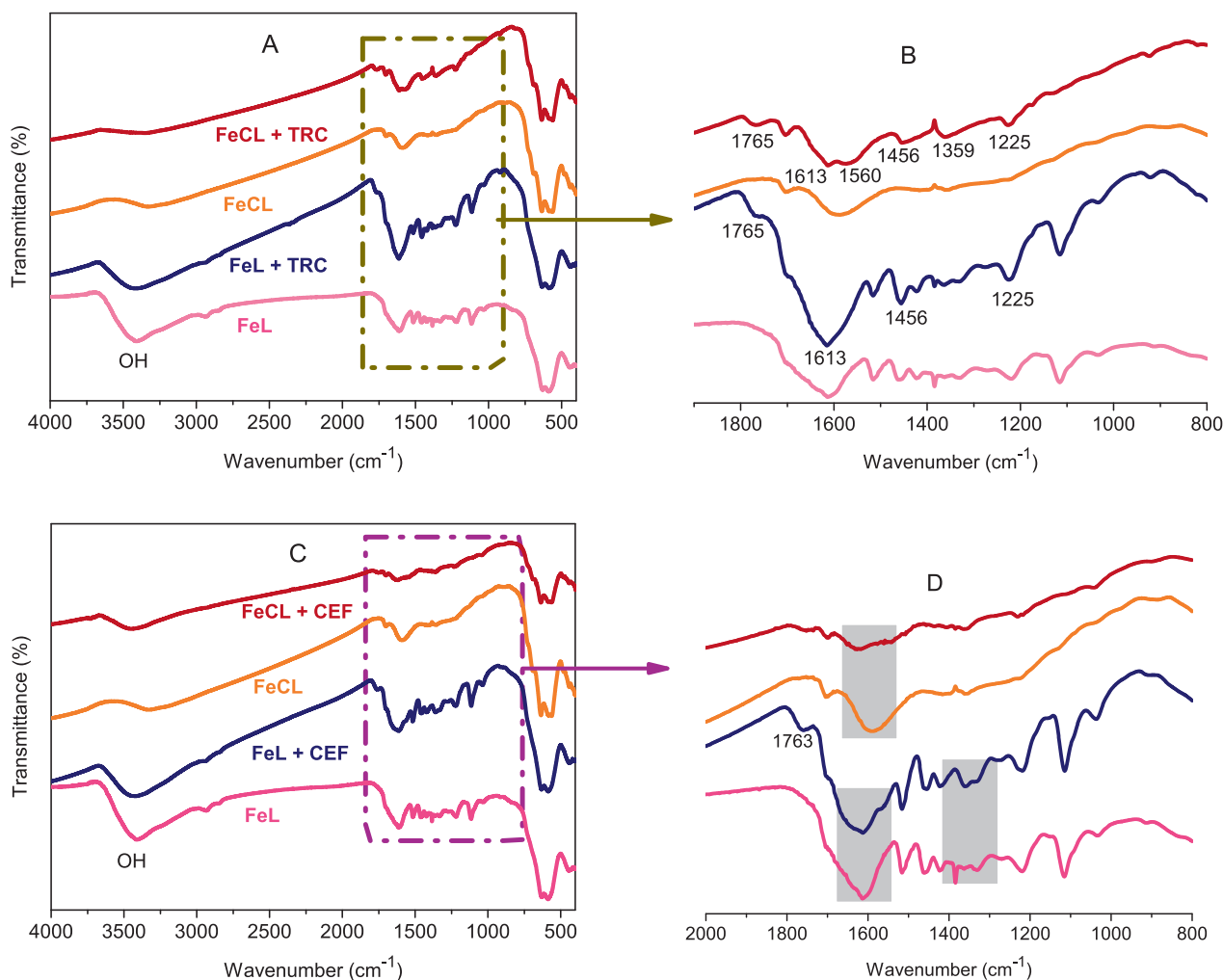


**Fig. 8.** The FTIR spectra of FeL and FeCL after the adsorption of TRC (A and B), and CEF (C and D).

### 3.8. DFT calculations on reactivity of tetracycline and ceftriaxone

Fig. 9A and B show the calculated frontier molecular orbitals while Fig. 10 shows the calculated Fukui dual descriptor surfaces for both TRC and CEF. We can see in Fig. 9A that the HOMO orbital of TRC is heavily localized around the tertiary amino group and therefore this group is more nucleophilic and should be preferential to undergo an electrophilic attack. This is better visualized in Fig. 10A where we can see that the more red areas are indeed around the amino group. The red surface areas in Fig. 10A have a larger contribution from the  $f^-(r)$  function and have more nucleophilicity, therefore are more likely to donate electron density. Thus, we can expect that this group should be able to receive hydrogen bonding through its nitrogen atom, but likely through the neighbor carbonyl oxygen as well, since this group is also mildly nucleophilic. This corroborates with previously mentioned IR results which show changes in the OH band of FeL.

Regarding the electrophilic areas, we can see that the central carbonyl group is the bluest region of the molecule, which also supports the previous hypothesis that this group may be involved in the main linkage between TRC and the adsorbents. One can see that the aromatic rings in the same way contain various different blue areas, corroborating with the assumption of  $\pi$ - $\pi$  interaction. It is worth to mention that both of these mentioned groups are also the ones involved in the LUMO orbital, complementing the results from the dual descriptor Fukui surfaces.

A similar qualitative reactivity analysis can be done for ceftriaxone observing the frontier orbitals and dual descriptor Fukui surface from Fig. 9A and B. The HOMO orbital is concentrated in the 5-atom ring (which contains sulfur and nitrogen) and the  $\text{NH}_2$ , reflecting that on the Fukui surface both groups are rather nucleophilic, and could be the ones interacting with groups like the C-H in lignin. On the other hand, the LUMO orbital surrounds the COOH group. However, as discussed before this group should be already deprotonated and reduced, and it is likely available for hydrogen bonding with lignin's OH groups, as shown in the IR spectra of FeL. Looking again at the dual descriptor Fukui surface in Fig. 10B, the other electrophilic areas are distributed along many other small groups in the molecule, together with also other nucleophilic areas. This mixed arrangement of nucleophilic and electrophilic groups along the molecule can favor general electrostatic or other non-covalent interactions with the proper stacking between CEF and FeL or FeCL, including  $\pi$ - $\pi$  interactions.

Based on the results obtained from the effect of pH, ionic strength, FTIR, and DFT, the adsorption mechanisms are summarized accordingly. The adsorption of TRC on FeL and FeCL followed the listed pattern - the electrostatic attraction (premise of pH study), hydrophobic interaction (shown during the ionic strength experiments), and  $\pi$ - $\pi$  interaction (FTIR results). The hydrogen bond interaction was observed for only FeL (FTIR results). The proposed adsorption mechanisms of CEF by FeL and FeCL are electrostatic attraction, hydrophobic interaction and  $\pi$ - $\pi$  interaction. The hydrogen bond interaction

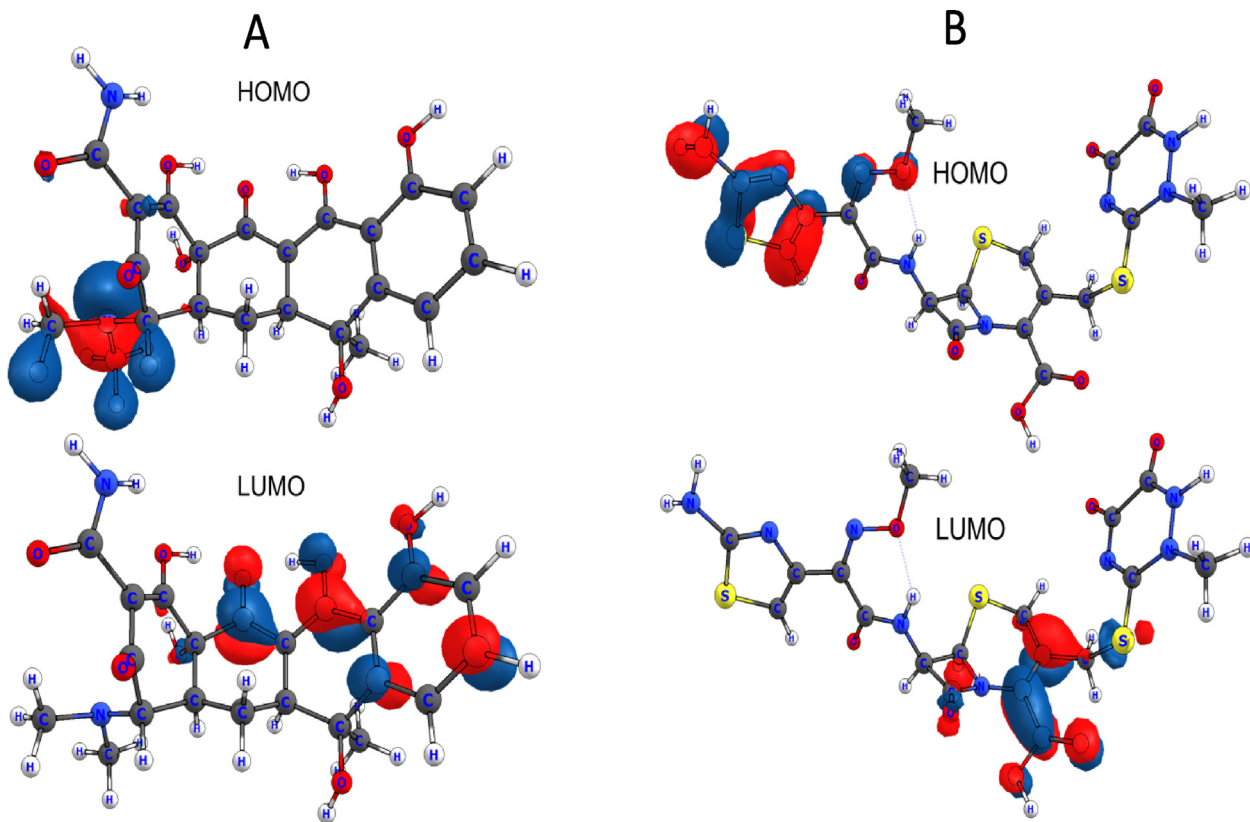


Fig. 9. Tetracycline B3LYP/def2-TZVPD frontier orbitals (A); Ceftriaxone B3LYP/def2-TZVPD frontier orbitals (B).

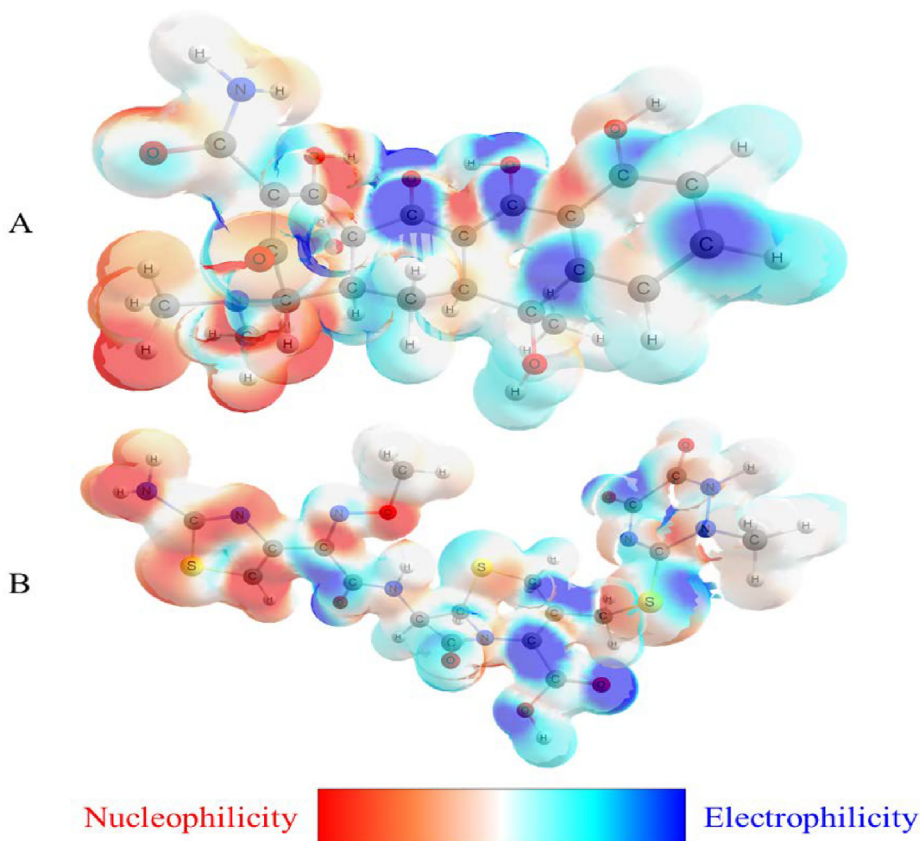


Fig. 10. Tetracycline (A) and ceftriaxone (B) dual descriptor Fukui function surfaces. While blue regions are more prone to undergo a nucleophilic attack, and are therefore more electrophilic, red regions are more prone to suffer an electrophilic attack, and are therefore more nucleophilic. (For interpretation of the references to color in this figure legend, the reader is referred to the web version of this article.)

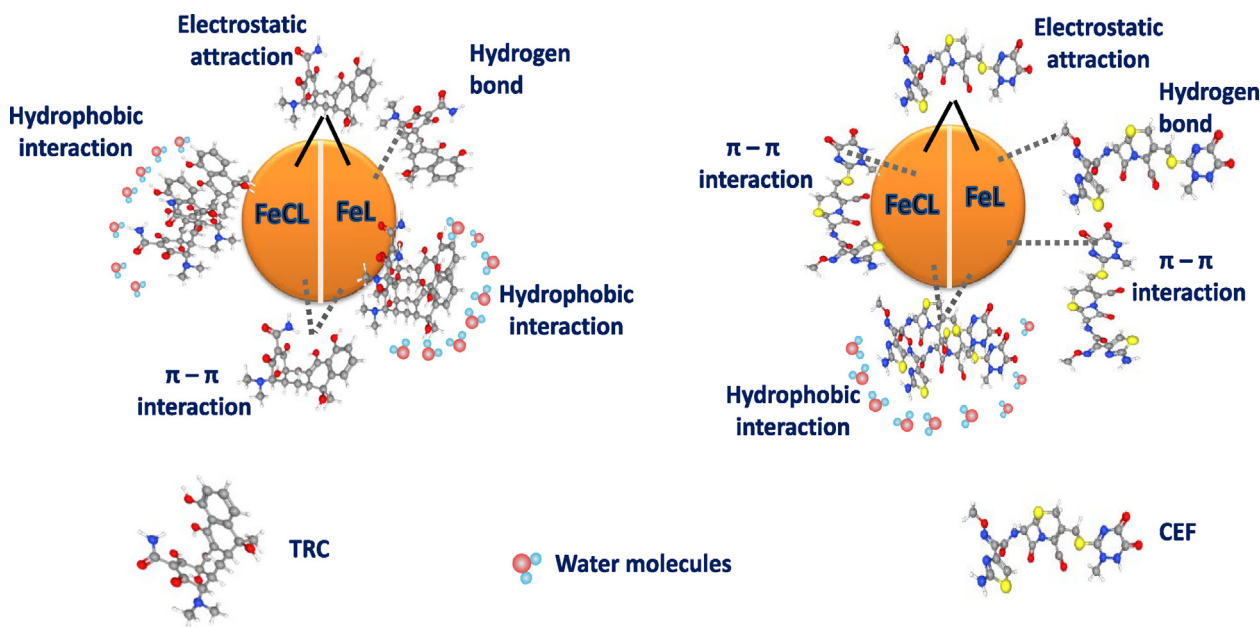


Fig. 11. The scheme of the proposed adsorption mechanism of TRC and CEF on FeL and FeCL.

was observed only in FeL. In summary the addition of hydrogen bond adsorption mechanism, that was noticed in FeL, is due to the abundant of hydroxyl group of lignin. These proposed mechanisms were consolidated by the DFT calculations. The scheme of the proposed adsorption mechanisms is displayed in Fig. 11.

### 3.9. Reusability and regeneration through thermal treatment

In this study, FeCL which had undergone thermal treatment was used. In this case, FeCL\_ adsorbed TRC and FeCL\_ adsorbed CET were thermal treated under nitrogen gas at 500 °C for 1 h. Nitrogen gas was chosen since it is inert to FeCL, and prevented the oxidation of both magnetite (Fe) and the carbonized lignin (CL). Prior to this, powder TRC and CET were separately thermal treated under the same condition as FeCL\_ adsorbed TRC and FeCL\_ adsorbed CET. Showing in Fig. 12A and B are the FTIR of TRC and CET before and after thermal treatment, which show the transformation of organic molecules to carbon materials, with respective change in color as shown in the insert photos. The spectra of both TRC\_ATT (after thermal treatment) and CET\_ATT (after thermal treatment) are similar to the spectra of carbonized materials [74,75]. With

this, discharging the thermally treated FeCL\_ adsorbed TRC and FeCL\_ adsorbed CET into environment will not constitute any hazard to the ecosystem. The results of the reusability of the thermally treated FeCL\_ adsorbed TRC and FeCL\_ adsorbed CET were shown in Fig. 12C. The reusability was carried out as follows: after adsorption of the respective antibiotics, the nanoparticles (FeCL) was separated from the supernatant, and thermally treated at 500 °C for the desorption (thermal degradation of TRC and CET). After which, the thermally treated FeCL was introduced into the fresh solution of the respective antibiotics of the same concentration as the first process. thermal treatment was again carried out after the adsorption process and reuse. This process continued for 3 cycles. The results up to 3 cycles show this material is economically viable. The amount of TRC adsorbed reduced from 71 (1st cycle) to 65 mg g<sup>-1</sup> (3rd cycle), while CET reduced from 83 (1st cycle) to 67 mg g<sup>-1</sup> (3rd cycle). Therefore, the recycling of the FeCL through thermal treatment, offers an opportunity for its reuse up to 3 cycles (as demonstrated in Fig. 12C), without an alarming reduction in its efficiency. As demonstrated by the TGA plot (Fig. S5), the mass loss of FeCL\_ adsorbed TRC and FeCL\_ adsorbed CET compare to FeCL was due to the presence of the loaded respective antibiotics.

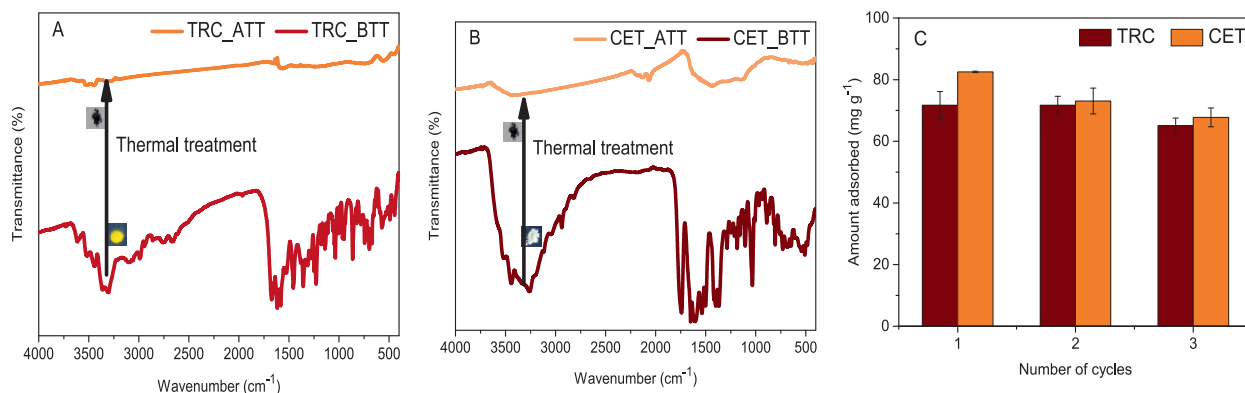


Fig. 12. FTIR of TRC (A), CET (B) before and after thermal treatment and the reusability of FeCL (C).

## 4. Conclusions

In this work, we synthesized super-paramagnetic composites (Fe<sub>3</sub>O<sub>4</sub>-lignin (FeL) and Fe<sub>3</sub>O<sub>4</sub>-lignin based carbon (FeCL)) for the removal of tetracycline (TRC) and ceftriaxone (CEF) from aqueous solutions. Morphological studies showed that the nanoparticles of both composites are spherical-like shapes. The BET specific surface area of FeCL was found to be 27 m<sup>2</sup>/g higher than FeL. No significant difference in the diffractogram of the two samples was noticed. The adsorption studies showed that pH of the solution and the presence of the competing ions, influence the removal of the targeted contaminants. Langmuir isotherm was found suitable to explain the adsorption process. While the adsorption of TRC was endothermic that of CEF was exothermic. The theoretical adsorption capacity estimated on the basis of Langmuir isotherm is about 156 and 148 mg g<sup>-1</sup> by FeL and FeCL respectively, for the removal of TRC, while it is almost the same in the case of CEF. Based on the experimental and computational studies, the adsorption mechanisms of TRC and CEF by FeL and FeCL are electrostatic attraction, hydrophobic, and  $\pi$ - $\pi$  interaction, while only FeL shows the addition of hydrogen bonds with both TRC and CEF. It was also found that FeCL can be reused for up to 3 cycles with little loss in its efficiency capacity.

## CRedit authorship contribution statement

**Olusegun Sunday J:** Conceptualization, Formal analysis, Validation, Investigation, Data curation, Writing – original draft, Writing – review & editing. **Osial Magdalena:** Validation, Writing – review & editing. **Taiane G.F. Souza:** Formal analysis, Writing – review & editing. **Michal Krajewski:** Formal analysis, Writing – original draft, Writing – review & editing. **Gabriel L.S. Rodrigues:** Formal analysis, Investigation, Writing – original draft, Writing – review & editing. **Pekala Marek:** Formal analysis, Validation, Writing – review & editing. **Krysinski Pawel:** Supervision, Project administration, Resources, Funding acquisition, Writing – review & editing.

## Data availability

Data will be made available on request.

## Declaration of Competing Interest

The authors declare that they have no known competing financial interests or personal relationships that could have appeared to influence the work reported in this paper.

## Acknowledgements

Sunday J. Olusegun with No PPN/ULM/2020/1/00051/DEC/01, would like to thank the NAWA - Narodowa Agencja Wymiany Akademickiej (Polish National Agency for Academic Exchange) for their support.

## Appendix A. Supplementary material

Supplementary data to this article can be found online at <https://doi.org/10.1016/j.molliq.2022.121075>.

## References

- [1] P. Zhu, D. Luo, M. Liu, M. Duan, J. Lin, X. Wu, Flower-globular BiO/BiVO<sub>4</sub>/g-C<sub>3</sub>N<sub>4</sub> with a dual Z-scheme heterojunction for highly efficient degradation of antibiotics under visible light, *Sep. Purif. Technol.* 297 (2022), <https://doi.org/10.1016/j.seppur.2022.121503>.
- [2] S.J. Olusegun, N.D.S. Mohalle, Insight into the adsorption of doxycycline hydrochloride on different thermally treated hierarchical CoFe<sub>2</sub>O<sub>4</sub> / bio-silica nanocomposite, *J. Environ. Chem. Eng.* 7 (6) (2019) 103442.
- [3] X. Wang, D. Ryu, R.H. Houtkooper, J. Auwerx, Antibiotic use and abuse: A threat to mitochondria and chloroplasts with impact on research, health, and environment, *BioEssays.* 37 (2015) 1045–1053, <https://doi.org/10.1002/bies.201500071>.
- [4] S.I. Polianciuc, A.E. Gurzău, B. Kiss, M. Georgia Ștefan, F. Loghin, Antibiotics in the environment: causes and consequences, *Med. Pharm. Reports.* 93 (2020) 231–240, <https://doi.org/10.15386/MPR-1742>.
- [5] V. Minden, A. Deloy, A.M. Volkert, S.D. Leonhardt, G. Pufal, Antibiotics impact plant traits, even at small concentrations, *AoB Plants.* 9 (2017), <https://doi.org/10.1093/aobpla/plx010>.
- [6] Z. Chu, B. Zheng, W. Wang, Y. Li, Y. Yang, Z. Yang, Magnetic Nitrogen-Doped biochar for adsorptive and oxidative removal of antibiotics in aqueous solutions, *Sep. Purif. Technol.* 297 (2022), <https://doi.org/10.1016/j.seppur.2022.121508>.
- [7] L. Herrera-Hidalgo, M.V. Gil-Navarro, S. Dilly Penchala, L.E. López-Cortes, A. de Alarcón, R. Luque-Márquez, L.F. López-Cortes, A. Gutiérrez-Valencia, Ceftriaxone pharmacokinetics by a sensitive and simple LC-MS/MS method: development and application, *J. Pharm. Biomed. Anal.* 189 (2020) 113484.
- [8] J. Gao, Y. Gao, Z. Sui, Z. Dong, S. Wang, D. Zou, Hydrothermal synthesis of BiOBr/FeWO<sub>4</sub> composite photocatalysts and their photocatalytic degradation of doxycycline, *J. Alloys Compd.* 732 (2018) 43–51, <https://doi.org/10.1016/j.jallcom.2017.10.092>.
- [9] K.K. Kefeni, B.B. Mamba, T.A.M. Msagati, Application of spinel ferrite nanoparticles in water and wastewater treatment: a review, *Sep. Purif. Technol.* 188 (2017) 399–422, <https://doi.org/10.1016/j.seppur.2017.07.015>.
- [10] T.N. Pham, T.Q. Huy, A.-T. Le, Spinel ferrite (AFe<sub>2</sub>O<sub>4</sub>)-based heterostructured designs for lithium-ion battery, environmental monitoring, and biomedical applications, *RSC Adv.* 10 (52) (2020) 31622–31661.
- [11] V. Zviagin, M. Grundmann, R. Schmidt-grund, Impact of defects on magnetic properties of spinel zinc ferrite thin films, *Phys. Status Solidi B.* 257 (2020) 1900630, <https://doi.org/10.1002/pssb.201900630>.
- [12] C.N. Lininger, C.A. Cama, K.J. Takeuchi, A.C. Marschilok, E.S. Takeuchi, A.C. West, M.S. Hybertsen, Energetics of lithium insertion into magnetite, defective magnetite, and maghemite, *Chem. Mater.* 30 (2018) 7922–7937, <https://doi.org/10.1021/acs.chemmater.8b03544>.
- [13] M. Usman, P. Faure, K. Hanna, M. Abdelmoula, C. Ruby, Application of magnetite catalyzed chemical oxidation (Fenton-like and persulfate) for the remediation of oil hydrocarbon contamination, *Fuel.* 96 (2012) 270–276, <https://doi.org/10.1016/j.fuel.2012.01.017>.
- [14] F. Keyhanian, S. Shariati, M. Faraji, M. Hesabi, Magnetite nanoparticles with surface modification for removal of methyl violet from aqueous solutions, *Arab. J. Chem.* 9 (2016) S348–S354.
- [15] H. Park, A. May, L. Portilla, H. Dietrich, F. Münch, T. Rejek, M. Sarcletti, L. Banspach, D. Zahn, M. Halik, Magnetite nanoparticles as efficient materials for removal of glyphosate from water, *Nat. Sustain.* 3 (2020) 129–135, <https://doi.org/10.1038/s41893-019-0452-6>.
- [16] A.A. Babaei, Z. Baboli, N. Jaafarzadeh, G. Goudarzi, M. Bahrami, M. Ahmadi, Synthesis, performance, and nonlinear modeling of modified nano-sized magnetite for removal of Cr (VI) from aqueous solutions, *Desalination Water Treat.* 53 (3) (2015) 768–777.
- [17] K. Ohe, Y. Tagai, S. Nakamura, T. Oshima, Y. Baba, Adsorption Behavior of Arsenic (III) and Arsenic (V) Using Magnetite, *J. Chem. Eng. Japan.* 38 (8) (2005) 671–676.
- [18] M. Ghaemi, G. Absalan, Fast removal and determination of doxycycline in water samples and honey by Fe<sub>3</sub>O<sub>4</sub> magnetic nanoparticles, *J. Iran. Chem. Soc.* 12 (2015) 1–7, <https://doi.org/10.1007/s13738-014-0450-6>.
- [19] D.H.K. Reddy, Y.S. Yun, Spinel ferrite magnetic adsorbents: alternative future materials for water purification?, *Coord. Chem. Rev.* 315 (2016) 90–111, <https://doi.org/10.1016/j.ccr.2016.01.012>.
- [20] N. Dudchenko, S. Pawar, I. Perelshtein, D. Fixler, Magnetite nanoparticles: synthesis and applications in optics and nanophotonics, *Materials (Basel).* 15 (2022) 1–34.
- [21] A. Niculescu, C. Chircov, A. Mihai, Magnetite nanoparticles: synthesis methods – a comparative review, *Methods.* 199 (2022) 16–27, <https://doi.org/10.1016/j.ymeth.2021.04.018>.
- [22] G. Fadillah, S.P. Yudha, S. Sagadevan, I. Fatimah, O. Muraza, Magnetic iron oxide/clay nanocomposites for adsorption and catalytic oxidation in water treatment applications, *Open Chem.* 18 (2020) 1148–1166, <https://doi.org/10.1515/chem-2020-0159>.
- [23] S. Laurichesse, L. Avérous, Chemical modification of lignins: towards biobased polymers, *Prog. Polym. Sci.* 39 (2014) 1266–1290, <https://doi.org/10.1016/j.progpolymsci.2013.11.004>.
- [24] R. Nad, H. Aleš, A. Lis, M. Jablonski, I. Šurina, V. Majov, A. Baco, Lignin modifications, applications, and possible market prices, *Energies* 15 (2022) 1–16.
- [25] H. Liu, H. Chung, Lignin-based polymers via graft copolymerization lignin-based polymers via graft copolymerization, *J. Polym. Sci.* 55 (21) (2017) 3515–3528.
- [26] S. Ma, F. He, D. Tian, D. Zou, Z. Yan, Y. Yang, T. Zhou, K. Huang, H. Shen, J. Fang, Variations and determinants of carbon content in plants: A global synthesis, *Biogeosciences.* 15 (2018) 693–702, <https://doi.org/10.5194/bg-15-693-2018>.

- [27] C. Chih-Hsin, J. Lehmann, J. Kinyangi, D. Solomon, T.-L. Wu, Long-term effects of black carbon on soil properties, 19th World Congr. Soil Sci. Soil Solut. a Chang World. (2010) 86–89. <http://www.cabdirect.org/abstracts/20113345983.html>.
- [28] G. Shrestha, S.J. Traina, C.W. Swanston, Black carbon's properties and role in the environment: a comprehensive review, *Sustainability*. 2 (2010) 294–320, <https://doi.org/10.3390/su2010294>.
- [29] D. Levy, R. Giustetto, A. Hoser, Structure of magnetite (Fe<sub>3</sub>O<sub>4</sub>) above the Curie temperature: a cation ordering study, *Phys. Chem. Miner.* 39 (2012) 169–176, <https://doi.org/10.1007/s00269-011-0472-x>.
- [30] A.D. Becke, Density-functional thermochemistry. III. The role of exact exchange Ab initio effective core potentials for molecular calculations. Potentials for K to Au including the outermost core orbitals Self-consistent molecular orbital methods. XX. A basis set for, *J. Chem. Phys.* 98 (1993) 448799–9982. Doi: 10.1063/1.472933.
- [31] C. Lee, W. Yang, R.G. Parr, Development of the Colle-Salvetti correlation-energy formula into a functional of the electron density, *Phys. Rev. B*. 37 (1988) 785–789, <https://doi.org/10.1103/PhysRevB.37.785>.
- [32] F. Weigend, R. Ahlrichs, Balanced basis sets of split valence, triple zeta valence and quadruple zeta valence quality for H to Rn: Design and assessment of accuracy, *Phys. Chem. Chem. Phys.* 7 (2005) 3297, <https://doi.org/10.1039/b508541a>.
- [33] D. Rappoport, F. Furche, Property-optimized Gaussian basis sets for molecular response calculations, *J. Chem. Phys.* 133 (2010), <https://doi.org/10.1063/1.3484283>.
- [34] C. Morell, A. Grand, A. Toro-Labbé, \*, ‡ Alejandro Toro-Labbé\*, New dual descriptor for chemical reactivity, *J. Phys. Chem. A*. 109 (1) (2005) 205–212.
- [35] J.I. Martínez-Araya, Why is the dual descriptor a more accurate local reactivity descriptor than Fukui functions?, *J. Math. Chem.* 53 (2015) 451–465, <https://doi.org/10.1007/s10910-014-0437-7>.
- [36] M.R. Snowdon, A.K. Mohanty, M. Misra, A study of carbonized lignin as an alternative to carbon black, *ACS Sustain. Chem. Eng.* 2 (2014) 1257–1263, <https://doi.org/10.1021/sc500086v>.
- [37] Y. Meng, C.I. Contescu, P. Liu, S. Wang, S.H. Lee, J. Guo, T.M. Young, Understanding the local structure of disordered carbons from cellulose and lignin, *Wood Sci. Technol.* 55 (2021) 587–606, <https://doi.org/10.1007/s00226-021-01286-6>.
- [38] M. Brebu, C. Vasile, Thermal degradation of lignin – a review, *Cellul. Chem. Technol.* 44 (2010) 353–363.
- [39] S. Nikafshar, O. Zabihi, Y. Moradi, M. Ahmadi, S. Amiri, M. Naebe, Catalyzed synthesis and characterization of a novel lignin-based curing agent for the curing of high-performance epoxy resin, *Polymers (Basel)*. 9 (12) (2017) 266.
- [40] R. Nandanwar, A. Chaudhari, J. Ekhe, Nitrobenzene oxidation for isolation of value added products from industrial waste lignin, *J. Chem., Biol. Phys. Sci.* 3 (2016) 501–513.
- [41] S.J. Olusegun, G. Larrea, M. Osial, K. Jackowska, P. Kryszewski, Photocatalytic degradation of antibiotics by superparamagnetic iron oxide nanoparticles, *Tetracycline Case, Catalysis*. 11 (2021) 1–18.
- [42] W.S. Peternele, V.M. Fuentes, M.L. Fascinelli, J. Rodrigues, R.C. Silva, C.M. Lucci, R.B. De Azevedo, Experimental investigation of the coprecipitation method: an approach to obtain magnetite and maghemite nanoparticles with improved properties, *J. Nanomater.* 2014 (2014) 1–10.
- [43] W. Zuo, N. Li, B. Chen, C. Zhang, Q. Li, M. Yan, Investigation of the deprotonation of tetracycline using differential absorbance spectra: a comparative experimental and DFT/TD-DFT study, *Sci. Total Environ.* 726 (2020), <https://doi.org/10.1016/j.scitotenv.2020.138432>.
- [44] M. Aleksić, V. Savić, G. Popović, N. Burić, V. Kapetanović, Acidity constants of cefetam, cefotaxime and ceftriaxone; the effect of the substituent at C3 position, *J. Pharm. Biomed. Anal.* 39 (2005) 752–756, <https://doi.org/10.1016/j.jpba.2005.04.033>.
- [45] P.S. Pinto, G.D. Lanza, M.N. Souza, J.D. Ardisson, R.M. Lago, Surface restructuring of red mud to produce FeO x (OH) y sites and mesopores for the efficient complexation / adsorption of  $\beta$ -lactam antibiotics, *Environ. Sci. Pollut. Res.* 25 (7) (2018) 6762–6771.
- [46] H.N. Tran, S.-J. You, A. Hosseini-Bandegharai, H.-P. Chao, Mistakes and inconsistencies regarding adsorption of contaminants from aqueous solutions: a critical review, *Water Res.* 120 (2017) 88–116, <https://doi.org/10.1016/j.watres.2017.04.014>.
- [47] V. Soares, M.C. Grando, G.L. Colpani, L.L. Silva, J. Maria, M. De Mello, Obtaining of Fe<sub>3</sub>O<sub>4</sub>@C core-shell nanoparticles as an adsorbent of tetracycline in aqueous solutions 2. Experimental procedure, *Mater. Res.* 22 (2019) 1–11.
- [48] J.i. Zang, T. Wu, H. Song, N. Zhou, S. Fan, Z. Xie, J. Tang, Removal of tetracycline by hydrous ferric oxide: adsorption kinetics, isotherms, and mechanism, *Int. J. Environ. Res. Public Health*. 16 (22) (2019) 4580.
- [49] H. Wang, C. Fang, Q. Wang, Y. Chu, Y. Song, Y. Chen, X. Xue, Sorption of tetracycline on biochar derived from rice straw and swine manure, *RSC Adv.* 8 (2018) 16260–16268, <https://doi.org/10.1039/c8ra01454j>.
- [50] X. Zhang, Y. Li, M. Wu, Y. Pang, Z. Hao, M. Hu, R. Qiu, Enhanced adsorption of tetracycline by an iron and manganese oxides loaded biochar: kinetics, mechanism and column adsorption, *Bioresour. Technol.* 320 (2021), <https://doi.org/10.1016/j.biortech.2020.124264>.
- [51] X. Zhang, X. Lin, Y. He, Y. Chen, X. Luo, R. Shang, Study on adsorption of tetracycline by Cu-immobilized alginate adsorbent from water environment, *Int. J. Biol. Macromol.* 124 (2019) 418–428, <https://doi.org/10.1016/j.ijbiomac.2018.11.218>.
- [52] X. Zhu, Y. Liu, F. Qian, C. Zhou, S. Zhang, J. Chen, Bioresource technology preparation of magnetic porous carbon from waste hydrochar by simultaneous activation and magnetization for tetracycline removal, *Bioresour. Technol.* 154 (2014) 209–214, <https://doi.org/10.1016/j.biortech.2013.12.019>.
- [53] A. Zaher, M. Taha, R.K. Mahmoud, Possible adsorption mechanisms of the removal of tetracycline from water by La-doped Zn-Fe-layered double hydroxide, *J. Mol. Liq.* 322 (2021), <https://doi.org/10.1016/j.molliq.2020.114546>.
- [54] B.M. Yegane, A. Azari, H. Pasalari, A. Esrafilii, M. Farzadkia, Modification of activated carbon with magnetic Fe<sub>3</sub>O<sub>4</sub> nanoparticle composite for removal of ceftriaxone from aquatic solutions, *J. Mol. Liq.* 261 (2018) 146–154, <https://doi.org/10.1016/j.molliq.2018.04.019>.
- [55] M.E. Mahmoud, A.M. El-ghanam, R.H.A. Mohamed, S.R. Saad, Enhanced adsorption of Levofloxacin and Ceftriaxone antibiotics from water by assembled composite of nanotitanium oxide / chitosan / nano-bentonite, *Mater. Sci. Eng. C*. 108 (2020), <https://doi.org/10.1016/j.msec.2019.110199>.
- [56] M. Dávila-Estrada, J.J. Ramírez-García, M.J. Solache-Ríos, J.L. Gallegos-Pérez, Kinetic and equilibrium sorption studies of ceftriaxone and paracetamol by surfactant-modified zeolite, *Water. Air. Soil Pollut.* 229 (2018), <https://doi.org/10.1007/s11270-018-3783-4>.
- [57] P.S. Pinto, G.D. Lanza, J.D. Ardisson, R.M. Lago, Controlled dehydration of Fe (OH)<sub>3</sub> to Fe<sub>2</sub>O<sub>3</sub>: developing mesopores with complexing iron species for the adsorption of  $\beta$ -lactam antibiotics, *J. Braz. Chem. Soc.* 30 (2019) 310–317, <https://doi.org/10.21577/0103-5053.20180179>.
- [58] M. Samarghandi, G. Asgari, R. Shokoohi, A. Dargahi, M. Moradi Golroki, H. Faraji, A. Arabkoushar, Efficiency of Saccharomyces Cerevisiae in Ceftriaxone Removal from Aquatic Environments: Kinetic, Isotherm of Adsorption and Thermodynamics Study, *J. Heal.* 10 (2019) 270–286. Doi: 10.29252/j.health.10.3.270.
- [59] S.J. Olusegun, N.D.S. Mohallem, V.S.T. Ciminelli, Reducing the negative impact of ceftriaxone and doxycycline in aqueous solutions using ferrihydrite / plant-based composites : mechanism pathway, *Environ. Sci. Pollut. Res.* (2022), <https://doi.org/10.1007/s11356-022-20561-y>.
- [60] M. El Kady, H. Shokry, H. Hamad, Effect of superparamagnetic nanoparticles on the physicochemical properties of nano hydroxyapatite for groundwater treatment: adsorption mechanism of Fe(II) and Mn(II), *RSC Adv.* 6 (2016) 82244–82259, <https://doi.org/10.1039/c6ra44497g>.
- [61] E.C. Lima, A. Hosseini-Bandegharai, J.C. Moreno-Piraján, I. Anastopoulos, A critical review of the estimation of the thermodynamic parameters on adsorption equilibria. Wrong use of equilibrium constant in the Van't Hoff equation for calculation of thermodynamic parameters of adsorption, *J. Mol. Liq.* 273 (2019) 425–434, <https://doi.org/10.1016/j.molliq.2018.10.048>.
- [62] F. Tomul, Y. Arslan, F. Turgut, Y. Babuçuo, H. Nguyen, Efficient removal of anti-inflammatory from solution by Fe-containing activated carbon : Adsorption kinetics , isotherms , and thermodynamics, 238 (2019) 296–306. Doi: 10.1016/j.jenvman.2019.02.088.
- [63] R. Attinti, D. Sarkar, K.R. Barrett, R. Datta, Adsorption of arsenic(V) from aqueous solutions by goethite/silica nanocomposite, *Int. J. Environ. Sci. Technol.* 12 (2015) 3905–3914, <https://doi.org/10.1007/s13762-015-0902-2>.
- [64] Y. Xiang, X. Yang, Z. Xu, W. Hu, Y. Zhou, Z. Wan, Y. Yang, Y. Wei, J. Yang, D.C.W. Tsang, Fabrication of sustainable manganese ferrite modified biochar from vinasse for enhanced adsorption of fluoroquinolone antibiotics: Effects and mechanisms, *Sci. Total Environ.* 709 (2020), <https://doi.org/10.1016/j.scitotenv.2019.136079>.
- [65] S.J. Olusegun, N.D.S. Mohallem, Comparative adsorption mechanism of doxycycline and Congo red using synthesized kaolinite supported CoFe<sub>2</sub>O<sub>4</sub> nanoparticles \*, *Environ. Pollut.* 260 (2020), <https://doi.org/10.1016/j.envpol.2020.114019>.
- [66] J. Kim, W. Li, B.L. Philips, C.P. Grey, Phosphate adsorption on the iron oxyhydroxides goethite ( $\alpha$ -FeOOH), akaganeite ( $\beta$ -FeOOH), and lepidocrocite ( $\gamma$ -FeOOH): A31P NMR Study, *Energy Environ. Sci.* 4 (2011) 4298–4305, <https://doi.org/10.1039/c1ee02093e>.
- [67] M. Zubair, M. Saood, M. Awwal, D. Pinto, L. Meili, W. Al, B. Essa, H. Al-adam, J. M. Alghamdi, N. Dalhat, S.A. Haladu, G. Khan, Production of magnetic biochar-steel dust composites for enhanced phosphate adsorption, *J. Water Process Eng.* 47 (2022), <https://doi.org/10.1016/j.jwpe.2022.102793>.
- [68] S. Yang, D. Ding, Y. Zhao, W. Huang, Z. Zhang, Z. Lei, Y. Yang, Investigation of phosphate adsorption from aqueous solution using Kanuma mud: Behaviors and mechanisms, *J. Environ. Chem. Eng.* 1 (2013) 355–362, <https://doi.org/10.1016/j.jece.2013.05.016>.
- [69] R.-y. Zhou, J.-X. Yu, H.-X. Li, R.-a. Chi, Removal of phosphate from aqueous solution by ferrihydrite/bagasse composite prepared through in situ precipitation method, *Colloids Surfaces A Physicochem. Eng. Asp.* 603 (2020) 125144.
- [70] S. Sudhakaran, E.V. Abraham, H. Mahadevan, K.A. Krishnan, Crosslinked chitosan-montmorillonite biocomposite with Fe intercalation: enhancing surface chemistry for improved phosphate adsorption, *Surfaces and Interfaces*. 27 (2021), <https://doi.org/10.1016/j.surfin.2021.101468>.
- [71] X. Qin, F. Liu, G. Wang, L. Weng, L. Li, Adsorption of levofloxacin onto goethite: Effects of pH, calcium and phosphate, *Colloids Surfaces B Biointerfaces*. 116 (2014) 591–596, <https://doi.org/10.1016/j.colsurfb.2013.09.056>.
- [72] J.T. McCue, Theory and Use of Hydrophobic Interaction Chromatography in Protein Purification Applications, in: *Methods Enzymol.*, 463rd ed., Methods in Enzymology, 2009: pp. 405–414.

- [73] H.N. Tran, S.J. You, T.V. Nguyen, H.P. Chao, Insight into the adsorption mechanism of cationic dye onto biosorbents derived from agricultural wastes, *Chem. Eng. Commun.* 204 (2017) 1020–1036, <https://doi.org/10.1080/00986445.2017.1336090>.
- [74] J. Rainer, V. Mrlik, R. Doris, H. Jakub, P. Sedlacek, B. Lucie, G. Soja, Biochar surface functional groups as affected by biomass feedstock, biochar composition and pyrolysis temperature, *Carbon Resour. Convers.* 4 (2021) 36–46, <https://doi.org/10.1016/j.crcon.2021.01.003>.
- [75] Y. Cuixia, X. Yingming, W. Lin, L. Xuefeng, S. Yuebing, Effect of different pyrolysis temperatures on physico-chemical characteristics and lead (II) removal of biochar derived from chicken manure †, *RSC Adv.* (2020) 3667–3674, <https://doi.org/10.1039/c9ra08199b>.